# Nanofabrication Using Electron Beam Lithography:

# Novel Resist and Applications

by

Arwa Abbas

A thesis

presented to the University of Waterloo

in fulfillment of the

thesis requirement for the degree of

Master of Applied Science

in

Mechanical Engineering - Nanotechnology

Waterloo, Ontario, Canada, 2013

© Arwa Abbas 2013

# AUTHOR'S DECLARATION

I hereby declare that I am the sole author of this thesis. This is a true copy of the thesis, including any required final revisions, as accepted by my examiners.

I understand that my thesis may be made electronically available to the public.

## ABSTRACT

This thesis addresses nanostructure fabrication techniques based on electron beam lithography, which is the most widely employed nanofabrication techniques for R&D and for the prototyping or production of photo-mask or imprint mold. The focus is on the study of novel resist and development process, as well as pattern transfer procedure after lithography.

Specifically, this thesis investigates the following topics that are related to either electron beam resists, their development, or pattern transfer process after electron beam lithography: (1) The dry thermal development (contrary to conventional solvent development) of negative electron beam resists polystyrene (PS) to achieve reasonably high contrast and resolution. (2) The solvent development for polycarbonate electron beam resist, which is more desirable than the usual hot aqueous solution of NaOH developer, to achieve a low contrast that is ideal for grayscale lithography. (3) The fabrication of metal nanostructure by electron beam lithography and dry liftoff (contrary to the conventional liftoff using a strong solvent or aqueous solution), to achieved down to ~50 nm resolution. (4) The study a novel electron beam resist poly(sodium 4-styrenesulfonate) (sodium PSS) that is water soluble and water developable, to fabricate the feature size down to ~ 40 nm. And finally, (5) The fabrication of gold nanostructure on a thin membrane, which will be used as an object for novel x-ray imaging, where we developed the fabrication process for silicon nitride membrane, electroplating of gold, and pattern transfer after electron beam lithography using single layer resist and tri-layer resist stack.

## ACKNOWLEDGEMENTS

I would like to express my heartfelt gratitude to Professor **Mustafa Yavuz** and Professor **Bo Cui** for supervising and making unlimited contributions to my work. Their tremendous enthusiasm and continual encouragement are powerfully reflected in this thesis. They have been ideal advisors who supported my efforts through thick and thin. It is my honour to acknowledge their support and encouragement as they provide a vast quantity of scientific insight, vitality, and inspiration to myself and within their work environments.

I would like to express my sincere appreciation to Professor **Bo Cui** for giving me reference letters, for his insightful conversations, ideas shared throughout the thesis's projects, knowledge, and logical way of thinking which have all had an extraordinary impact on my academic work. Professor **Bo Cui** provided a significant amount of theoretical and experimental insight into this work. Moreover, I thank Professor **Mustafa Yavuz** who offered his wisdom and guidance. His contributions have been of great worth in this thesis. Professor. **Bo Cui** trained me very well in the area of nanofabrication. Professor **Mustafa Yavuz** provided instructions and useful feedback and kept track of my progress to achieve high productivities.

Knowledge of the following talented graduate students in our group has been passed down to me over the last two years: **Celal Con**, **Jian Zhang**, **Ripon Kumar Dey**, **Xiangcheng,** and **Medhat Samaan**. These fellow students had the patience to clarify information and make initial contributions to my work with a steady current of support and clear thinking through discussion and sharing of ideas. I have found these contributions during daily lab work, in our group meetings, and within our thesis and publications to be of great utility and usefulness.

I owe my deepest gratitude to Professor **Zain Hassan Abdallah Yamani** the Director of the KFUPM Center of Excellence in Nanotechnology at King Fahd University of Petroleum and Minerals. I am extremely privileged to receive his continuous questions about my academic progress which strongly encouraged me to be more ambitious, motavaited, and eager.

I am deeply grateful to Eng'r. **Abdullah Mohammed**, a chemical engineer previously at the Saudi Arabian Oil Company (Saudi Aramco). His extreme intelligence, enthusiasm, and continual support are strongly reflected in my performance. His inspiration is helpful and beneficial in enabling me to be well-focused to serve and assist in developing our country with my knowledge and expertise through concentration, study, and broad perspective.

My sincere thanks to Richard Barber and Robert Mullins at the Giga-2 Nano lab; Nathan Nelson-Fitzpatrick, Brian Goddard, and Rodello (Rod) Salandanan at Quantum Nano Fabrication Facility; Professor Ting Tsui at the department of Chemical Engineering; and his student Brandon Seo. I have been fortunate to work in the Giga-2 Nano lab, Quantum Nano Fabrication Facility, and Ting's lab for scanning electron microscopy in a fruitful, safe and secure environment that keeps the facility running with their continued assistance for students.

I express a very special thanks to **Yusuf Saleh** at Saudi Arabia Royal Guard in Units of the Royal Guard. Yusaf Saleh provides incredible support to me with his valuable advice and great focus on obtaining the highest level of education linked with unique qualification, expertise, and dexterity. Special thanks are required for my dear friend **Somaih Mohammed** in KSA, who is always keeping in touch with me and has helped me overcome any obstacles and difficulties by assisting in these matters that I faced and providing me with wise suggestions to handle them. Thanks for her patience, understanding, support, and especially her care.

I would also like to thank my younger brother **Abdullah Saud**, an undergraduate in Nanotechnology engineering program at University of Waterloo. He is not just a brother but a very special and close friend of mine over the last two years during our time staying together in Canada. Thanks for his patience, understanding, support, and especially for his incredible care as he tries to follow our father's manner and attitude.

Dr. **Andrew Brzezinski,** and Dr. **Guoxing Miao** critically read and review this thesis in depth. The quality and accuracy of my thesis has been enhanced considerably thanks to their efforts.

Special thanks to **Xiangcheng**, with, whom I shared beneficial conversations and discussions. He offers for all the group valuable comments, feedback, and insight into the research. He is active and motivated and with his enthusiasm he inspired me to keep my work up to good standards. I am indebted to my friends, mentors, and advisors who helped me on this path of my master's study.

This work was supported by Saudi Ministry of Higher Education's financial funding (Saudi Culture Bureau in Canada), which provided me with a scholarship.

Finally, I am significantly indebted to my intelligent brothers and sisters who are enthusiastic and eager to learn new knowledge whether related or not to their fields; also, I am indebted to my great and distinguished **Mother** for her dedication, devotion, encouragement, faith, and love. She is my most powerful source of motivation and she has provided me with the strength to persist in completing this work well. I strongly offer my whole family the utmost appreciation for the loving support that I have received.

Moreover, the ever-present inspiration, strengthening, and prompting that I received from my **Father** before he passed away has not gone unnoticed.

# Dedication

To my great family

# Table of Contents

**AUTHOR'S DECLARATION** ........ **II**

**ABSTRACT** ........ **III**

**ACKNOWLEDGEMENTS** ........ **IV**

**DEDICATION** ........ **VII**

**LIST OF FIGURES** ........ **X**

**LIST OF TABLES** ........ **XIII**

**CHAPTER 1: HIGH RESOLUTION ELECTRON BEAM LITHOGRAPHY** ........ **1**
1.1 OVERVIEW OF NANOFABRICATION ........ 1
1.2 ELECTRON BEAM LITHOGRAPHY ........ 3
1.2.1 Instrumentation ........ 4
1.2.2 Overview of Electron Beam Sources ........ 5
1.2.2.1 Thermionic Emission ........ 6
1.2.2.2 Field Emission Source (Schottky Source) ........ 7
1.2.2.3 Cold Field Emission Source ........ 8
1.2.3 Limitations on Electron Beam Spot Size ........ 8
1.2.4 Electron Scattering and Proximity Effect ........ 10
1.2.5 EBL Resists ........ 12

**CHAPTER 2: DRY THERMAL DEVELOPMENT OF NEGATIVE ELECTRON BEAM RESISTS POLYSTYRENE (PS).** ........ **16**
2.1 INTRODUCTION ........ 16
2.2 EXPERIMENTAL DETAILS ........ 17
2.3 RESULTS AND DISCUSSION ........ 18
2.4 CONCLUSION ........ 21

**CHAPTER 3: POLYCARBONATE ELECTRON BEAM RESIST USING SOLVENT DEVELOPER** ........ **22**
3.1 INTRODUCTION ........ 22
3.2 EXPERIMENTAL ........ 23
3.3 RESULT AND DISCUSSION ........ 24
3.4 SUMMARY ........ 28

**CHAPTER 4: METAL NANOSTRUCTURE FABRICATION BY ELECTRON BEAM LITHOGRAPHY AND *DRY* LIFTOFF** ........ **29**
4.1 INTRODUCTION ........ 29
4.2 DRY LIFTOFF ........ 30
4.3 DRY LIFTOFF USING POLYCARBONATE (PC) RESIST ........ 31
4.3.1 Reason for Using Polycarbonate ........ 31
4.3.2 Experimental Details ........ 31
4.3.3 Results and Discussion ........ 32
4.4 DRY LIFTOFF USING BI-LAYER POLYCARBONATE AND PMGI ........ 33
4.4.1 Reason for Bi-layer ........ 33
4.4.2 Experiment Details ........ 34
4.4.3 Results and Discussion ........ 34
4.5 DRY LIFTOFF USING PMMA RESIST ........ 35
4.5.1 Reason for Using PMMA ........ 35
4.5.2 Experiment Details ........ 35
4.5.3 Results and Discussion ........ 36

4.5.4 Conclusion ........ 37

**CHAPTER 5: WATER SOLUBLE AND DEVELOPABLE ELECTRON BEAM RESIST PSS ........ 38**

5.1 INTRODUCTION ........ 38
5.2 EBL OF PSS COATED ON BARE SILICON WAFER ........ 38
5.3 EBL OF PSS COATED ON PMMA/SI ........ 38
5.4 EBL OF PSS COATED ON ARC/SI ........ 39
5.5 CONCLUSION ........ 41

**CHAPTER 6: FABRICATION OF MEMBRANE-SUPPORTED GOLD NANOSTRUCTURE FOR X-RAY IMAGING ........ 42**

6.1 INTRODUCTION ........ 42
6.2 X-RAY IMAGING BY BORRMANN PYRAMID ........ 43
6.3 STRUCTURE DESIGN AND ITS FABRICATION ........ 44
6.4 FABRICATION OF SILICON NITRIDE MEMBRANE ........ 45
6.4.1 Fabrication Principle ........ 45
6.4.2 Fabrication Steps ........ 45
6.4.3 Fabrication Results ........ 46
6.5 FABRICATION OF AU NANOSTRUCTURE ON MEMBRANE ........ 47
6.5.1 GOLD ELECTROPLATING ........ 47
6.5.1.1 Advantage of Electro-Deposition ........ 47
6.5.1.2 Electroplating Setup and Experimental Details ........ 47
6.5.1.3 Results of Electroplating ........ 49
6.5.2 GOLD STRUCTURE FABRICATION STEPS USING A SINGLE LAYER RESIST ........ 49
6.5.2.1 Results Using a Single Layer Resist ........ 50
6.5.3 FABRICATION STEP USING TRI-LAYER STACK ........ 51
6.5.4 CONCLUSION ........ 53

**APPENDIX: LIST OF PUBLICATIONS ........ 54**

**BIBLIOGRAPHY ........ 55**

## List of Figures

Figure 1-1: Schematic of (a) positive and (b) negative resists. ........................................ 4

Figure 1-2: Lift-off technique. ........................................................................................ 4

Figure 1-3: Scheme of components of an electron beam lithography system. [15] ............... 5

Figure 1-4: A typical electron gun with a thermionic source. ........................................... 6

Figure 1-5: Interaction of electrons (forward and backward scattered) with resist-coated wafer ......................................................................................................................... 11

Figure 1-6: Patterns created by normal and additional exposure. .................................. 11

Figure 1-7: Double Gaussian model describing the scattering of electrons from a finite size source [26] ............................................................................................................... 12

Figure 1-8: SEM images of 35 nm half-pitch PMMA and ZEP gratings exposed with 10 keV electrons and developed in ZED-N50, MIBK:IPA 1:3, and IPA: water 7:3 developers. The doses and minimum gap-widths achieved for each combination are noted. ......................................................................................................................... 14

Figure 1-9: Chemical formula for polystyrene ............................................................... 14

Figure 1-10: SEM image of 300nm period hole array exposed in ZEP resist .................. 15

Figure 1-11: SEM image of 300nm period pillar array after liftoff and RIE ................... 15

Figure 2-1: Contrast curves exposed at 20 keV for (a) 1.2 kg/mol polystyrene thermally developed at 250°C for 120 min; and (b) 2 kg/mol polystyrene developed at 350°C for 30min. ......................................................................................................................... 19

Figure 2-2: Dense periodic line arrays exposed at 20 keV and 96 pA beam current in 2 kg/mol polystyrene thermally developed at 350°C for 30min. (a) 200 nm pitch, 50 nm line-dose; (b) 100 nm pitch; and (c) 60 nm pitch. Line dose was 200 nC/cm. ................. 20

Figure 2-3: Contrast curves for 1.2kg/mol polystyrene exposed at 5 keV and developed first in xylene for 30 sec (diamond), and then thermally at 250°C for 4 hours (square). The absolute (triangle) and relative (circle) thickness change due to thermal development are also shown for doses that led to non-zero remaining thickness after thermal development. The relative change is defined as the ratio of absolute thickness change and average thickness before and after thermal development. ............................................... 21

Figure 3-1: (a) Chemical structure of bisphenol A polycarbonate; (b) Contrast curve for polycarbonate exposed at 20 keV and developed by cyclopentanone : IPA = 1:3 for 1 min, with the dose in log-scale; and (c) Same as (b) but with dose in linear-scale. ......... 25
Figure 3-2: Contrast curve for polycarbonate exposed at 20 keV and developed by xylene: IPA = 1:3 for 1 min, with dose in log-scale (a) and linear-scale (b). The xylene is p-, m-, o- mixed. ........................................................................................................ 26
Figure 3-1: Contrast curve for polycarbonate exposed at 20 keV and developed by pentyl acetate : IPA = 1:3 for 0.5 min, with dose in log-scale (a) and linear-scale (b). .............. 27
Figure 3-2: SEM image of line array pattern exposed in PC at 20 keV and developed by cyclopentanone (diluted with IPA at 1:3 volume ratio). The line width is close to 50 nm and array period is 1000 nm........................................................................................ 28
Figure 4-1: Schematic liftoff and direct etch method for pattern transfer, here transferring the polymer resist pattern into metal pattern.................................................................. 30
Figure 4-2: Metal lift-off process [11], (a) Ideal resists profile, (b) Deposition of metal, and (c) After lift-off.............................................................................................................. 31
Figure 4-3: SEM image of a stack of PC on silicon wafer created by e-beam writing at 20 keV; using a 1:3 mixture of cyclopentanone and 2-propanol; and after dry lift off process; a) Zoom-in scan to show the edge; b) Zoom-in scan of two squares an array, c) Zoom-out scan of an array. .............................................................................................................. 32
Figure 4-4: Process using PC/PMGI bi-layer resist for dry liftoff .................................. 33
Figure 4-5: SEM image of 10 nm-thick Cr pattern fabricated by dry liftoff, with poorly defined square pattern. .................................................................................................... 34
Figure 4-6: Photograph showing the peeling off process of the resist film using scotch tape ................................................................................................................................. 36
Figure 4-7: SEM images of Cr patterns fabricated by electron beam lithography and dry liftoff, (a) Line array with 56 nm line-width; and (b) Large squares having doses increasing exponentially from lower left to upper right. ................................................ 36
Figure 5-1: PSS on PMMA to solve the adhesion issue of PSS to silicon. ...................... 39
Figure 5-2: Contrast curve for sodium PSS exposed at 20keV and developed in DI water for 10 sec. The sensitivity ($D_{50}$) and contrast are derived as 2800 μC/cm2 and 0.8,

respectively. Also shown are the chemical structure of the resist and AFM image of the large (5μm by 5μm) exposed square array used to generate the contrast curve. .............. 40
Figure 5-3: High resolution pattern in sodium PSS by electron beam lithography at 20 keV. (a, c) Line array with line-width ~50 nm and pitch 400 nm. Narrower lines were found collapsed. (b, d) Pillar array with diameter 40 nm or 60 nm and height close to 150 nm. Again the smaller pillars fell off cue to capillary force during developer drying. (e, f) Zoom out view of the line array exposed at different doses. Too low dose resulted in narrow lines that fell off; whereas too high dose resulted in merged lines (upper part in (e)) due to over-exposure. ........................................................................................ 41
Figure 6-1: The popular x-ray imaging method using zone-plate lens. ........................... 42
Figure 6-2: Three triangles can be observed simultaneously on a single frame when two sets of atomic planes of a beryllium single crystal are excited. ....................................... 43
Figure 6-3: Linear absorption coefficient of Au. ............................................................ 44
Figure 6-4: The structure to be fabricated consisting of Au nanostructure (periodic array with 600 nm pitch) on top of a silicon nitride membrane. ............................................... 45
Figure 6-5: Silicon nitride membrane fabrication process. .............................................. 46
Figure 6-6: Photo of the metal shadow mask. Each repeating cell has a size of 5 mm, and the opening is 1.5 mm by 1.5 mm. ........................................................................ 46
Figure 6-7: $Si_3N_4$ membrane etched on a (100) silicon wafer using KOH etch. The array periodicity is 5 mm. ........................................................................................... 47
Figure 6-8 Schematic representation of electroplating process to fill holes in the resist. 48
Figure 6-9: I-V curve of the gold electroplating solution (by Golam Bappi). .................. 49
Figure 6-10: Photo of two pieces of wafer with electroplated gold on the Pt conducting layer. ........................................................................................................................ 49
Figure 6-11: Fabrication process steps using a single layer resist .................................... 50
Figure 6-12: SEM images polystyrene pattern on membrane showing collapsed patterns due to capillary force. ........................................................................................... 51
Figure 6-13: Fabrication process using tri- layer stack to create the polymer matrix for subsequent gold electroplating. ........................................................................... 52
Figure 6-14: SEM images of the result after pattern transfer into the tri-layer stacks...... 53

# List of Tables

Table 1-1: Capabilities of nanofabrication techniques based on the majority of reported findings ........ 2

Table 1-2: Characteristics of different types of electron sources ........ 5

Table 1-3: Popular e-beam resists and their properties ........ 13

# CHAPTER 1: High Resolution Electron Beam Lithography

## 1.1 Overview of Nanofabrication

Nanofabrication is the technology to produce nanoscale structures with dimensions down to sub-100nm.[1] It plays a critical role in all the fields of nanotechnologies.[1] Broadly speaking, there are two types of nanofabrication approaches: bottom-up and top down. The former is based on chemical synthesis of nanoparticles (nanoscale particles, wires, tubes, and other shapes like cones, and cages) and self-assembly of nanoscale blocks into ordered array of structures, and includes nano-sphere lithography, template-based methods that exploit nanoporous membranes (notably anodized alumina), self-assembly of block copolymers,[2, 3, 4, 5, 6, 7] self-assembly of atoms and molecules, and supramolecular elements.

Top-down fabrication techniques involve the manipulation of structures of bulk materials by eliminating or adding nanoscale patterns. The lateral size is determined by the lithography process, whereas the vertical one by thin film deposition and etching techniques. Nano-lithography techniques include ion beam lithography, electron beam lithography (EBL), nanoimprint, and scanning probe lithography. Top-down fabrication techniques are utilized for many applications including the semiconductor, digital and memory integrated circuits (ICs), information storage, photonics, and microfluidics.[1]

Lithography comprises a flow and transfer of the pattern information to a sensitive material by exposure that normally starts with the design of a pattern in the arrangement of a dataset.[8] Lithography is the most essential top-down fabrication technique that is critically paramount in many areas of modern science and technology with applications ranging from the fabrication of ICs devices to the fabrication of micro and nano electromechanical systems (MEMS, NEMS).

There are two types of lithography techniques. The first type duplicates the pattern of the mask, including optical lithography or charged particle projection lithography, x-ray

lithography[5] (XRL), extreme ultra-violet lithography[5] (EUVL) and nanoimprint lithography [6] (NIL). The second type is direct patterning that generates the pattern, including electron beam lithography (EBL),[9,10] ion beam lithography (IBL), scanning probes [5] (SPL), and electron-beam-induced deposition (EBID). [1] Apparently the first type has high throughput as the pattern over an entire mask or mold is duplicated in one step, thus it is suitable for high volume production. The second type generates pattern in a serial manner, thus it has low throughput and is suitable for R&D or the production of mask or mold used by the first type.

Optical lithography is the main lithography method used for semiconductor manufacturing and other production environment, owning to its high throughput and low cost. It can generate sub-100nm resolution. Moreover, high numerical aperture optics (immersion lithography) and Resolution Enhancement Techniques (RET) are used such as Off-Axis Illumination (OAI), Phase Shift Masks (PSM), Optical Proximity Correction (OPC), and double processing, [11, 12] which enhance the resolution down to sub-10 nm scale.

| **Technology** | **Capability** |
| --- | --- |
| Optical lithography | ~30nm |
| Electron beam lithography | ~10nm |
| Nanoimprint lithography | ~10nm |
| Scanning probe lithography | ~20nm |
| Focused ion beam | ~30nm |

Table 1-1: Capabilities of nanofabrication techniques based on the majority of reported findings [1]

Nanoimprint lithography is a simple nanolithography process with low cost, high throughput and high resolution. It creates patterns by mechanical deformation of imprint resist and subsequent processes. The imprint resist is typically a monomer or polymer formulation that is cured by heat or UV light during the imprinting. The most straightforward form of nanoimprint lithography is the hot embossing of a thermoplastic polymer thin film. The resolution is no longer limited by light diffraction as is the case for optical lithography, or charged beam scattering as is the case for electron beam

lithography. Therefore, there is no fundamental resolution limit for nanoimprint lithography, and the achievable resolution depends only on the mold resolution. For instance, a mold consisting of single wall carbon nanotube has been duplicated by nanoimprint lithography, which demonstrates a resolution down to 2 nm, higher than any other lithography methods except those based on scanning probe manipulation (atomic resolution).

**1.2 Electron Beam Lithography**

E-beam lithography (EBL) is a procedure by which a pattern is defined on a sample surface and is achieved by exposing a radiation sensitive resist with electrons. After development the resist pattern is transferred to the substrate by etching or liftoff methods. In this work EBL was utilized extensively; thus, the focus of this first chapter will be on the working principle of EBL that leads to high resolution features.

EBL is the main direct write technique for high resolution fabrication of nanoscale structures.[13] EBL procedures involve the spin-coating of the sensitive layer of e-beam resist on a substrate followed by the exposure of a beam of electrons that produces a chemical change in both positive and negative resists (see Figure 1-1). After electron beam exposure the chemistry of positive resists results in polymer chain scission, reducing the polymer chain length; therefore, the exposed area in resist is more easily dissolved in developer than the unexposed resist. After electron beam exposure the chemistry of negative resists of the exposed areas become cross-linked with the polymer chains; therefore, it is more difficult to dissolve the cross-linked polymer in developer. In other words, the exposed areas in the resists are dissolved in positive resists and remain in negative resists.[14] The developed pattern can be utilized for pattern transfer processes such as lift-off (see Figure 1-2) or etching. [15]

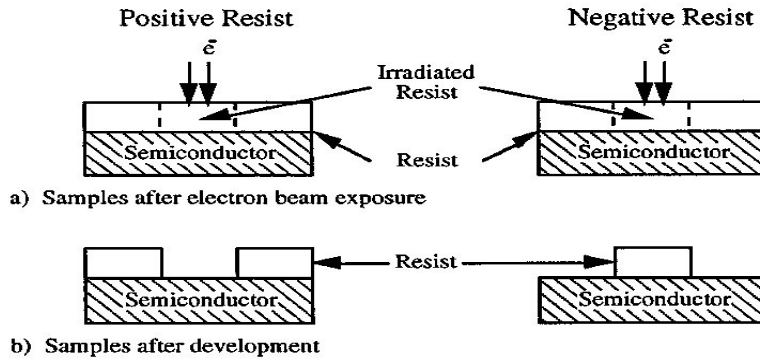


Figure 1-1: Schematic of (a) positive and (b) negative resists. [15]

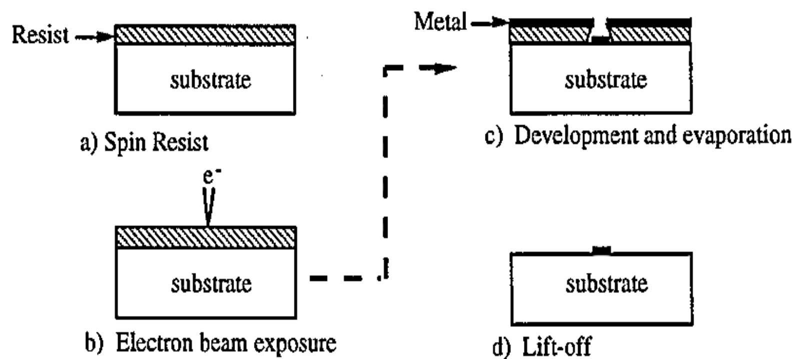


Figure 1-2: Lift-off technique. [15]

### 1.2.1 Instrumentation

Figure 1-3 shows a schematic of an electron beam lithography system. Generally, EBL technique involves the generation of electrons from the source that are subsequently accelerated to a desired energy and focused onto the resist surface to expose it. The electron gun that creates the electrons contains a cathode and beam shaping electrode. The required accelerations of emitted electrons beam ranging from 10 to 30 keV occur in the region between the cathode and the anode. The flow of beam is shaped and deflected by magnetic electron lens. The beam blanker is to blank the beam to avoid any exposure when the beam is in transit from one pattern element to anther.

The main purpose for maintaining the complete column from the electron gun to the wafer stage under high vacuum is to prevent the electron's trajectory from being influenced by the electrons' collision against gas molecules. [16] The computer and pattern generator determines how the beam scans on the resist surface according to pre-defined

CAD pattern file and exposure condition (dose, step size, etc.)

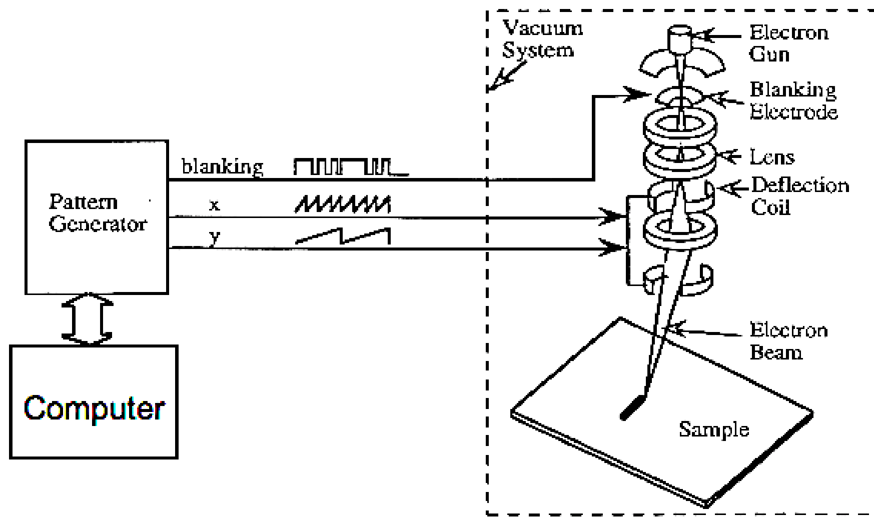


Figure 1-3: Scheme of components of an electron beam lithography system. [15]

### 1.2.2 Overview of Electron Beam Sources

| Source type / Working principle | Filament material | Brightness ($A/cm^2/rad$) | Source size | Energy dispersion (eV) | Vacuum level (Torr) | Filament temperature (K) |
|---|---|---|---|---|---|---|
| Tungsten thermoionic | W | $\sim 10^5$ | 25 μm | 2-3 | $10^{-6}$ | ~3000 |
| $LaB_6$ thermoionic | $LaB_6$ | $\sim 10^6$ | 10 μm | 2-3 | $10^{-8}$ | ~2000-3000 |
| Thermic field emission (Schottky) | Zr/O/W | $\sim 10^8$ | 20 nm | 0.9 | $10^{-9}$ | ~1800 |
| Cold field emission | W | $\sim 10^9$ | 5 nm | 0.22 | $10^{-10}$ | Ambience |

Table 1-2: Characteristics of different types of electron sources [17]

There are a variety of common electron beam sources such as thermal ionic (tungsten filament, and $LaB_6$ filament), thermal field emission filament, and cold field emission filament. Table 1-2 presents characteristics of different types of filaments utilized in the gun sources. [17]

#### 1.2.2.1 Thermionic Emission

The conductive materials (such as tungsten filaments, or $LaB_6$ filament) of the thermic sources receive heat for electron emission. Thermal field emission source consists of a tungsten filament, which is covered by a zirconium oxide layer. The filament emits electrons, while the covering layer decreases the work function (from 4.6 to 2.48 eV).

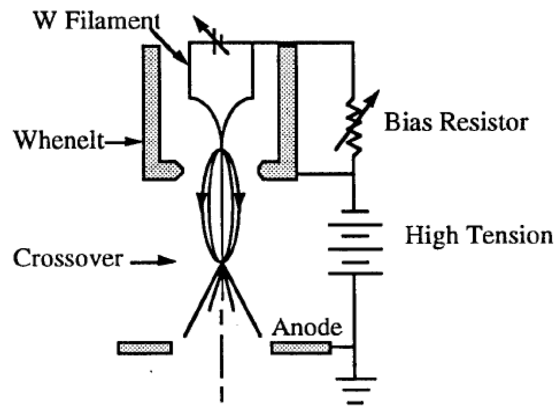


Figure 1-4: A typical electron gun with a thermionic source.

Figure 1-4 shows the common electron source that emits electrons by thermionic emission. The current source is for heating the tungsten filament to roughly 3000K, and the gun consists of a Whnelt electrode, which electrostatically focuses the emitted electrons to a crossover point. The crossover point is typically $10\mu$m in diameter and is focused by subsequent electron lens to demagnify the crossover point formed by the electron gun and project it onto the resist surface.

The focus characteristic used to evaluate an electron source is its brightness ($\beta$), which is the current emitted per unit area per unit solid angle. Brightness defines the maximum current density one can attain at the plane of image. For thermionic emission the brightness can be shown as: [15]

$$\beta = J_0 \frac{(-q)\Phi}{K_B T}$$

***Where:*** $J_o$: is the peak current density at the crossover

q: is the electron charge

$\phi$: is the accelerating potential in volts

$K_B$: is Boltzman's constant

T: is the emitter temperature

The brightness determines the maximum current density that can be attained at the image plane, and the current density in the focused spot at the image plane, $J_i$, is limited by the Langmuir equation. [18]

$$J_i = J_0 \frac{(-q)\Phi}{K_B T} \alpha^2 = \pi\beta\alpha^2$$

***Where:*** $\alpha$ is the semi-angle of convergence of the beam.

The purpose in achieving a semi-angle of convergence as small as possible is to reduce chromatic and spherical aberrations, and to attain the increases of source brightness of the current density at the image plane. As an example, brightness of tungsten (W) thermionic emitters operating at 40 kV is approximately 2 x $10^5$ A/cm$^2$/rad.

**1.2.2.2 Field Emission Source (Schottky Source)**

Though Schottky source is often referred as field emission source, it is actually thermionic source. The tip (filament) is heated to nearly 2000$^o$C, and there will be no emission (due to tunneling) when the heat is turned off. The main difference from regular thermionic emission is that the tip is sharp, thus the electric field at the sharp apex is very high, which lowed the energy barrier to become significantly smaller than the work function of the tip material. This increases the emission current drastically since the emission current depends on the energy barrier height exponentially. This high current combined with small filament apex (thus small virtual source size) lead to very high brightness compared to the regular thermionic filament. However, to avoid arc-over at the apex where electric field is the highest, very high vacuum is needed. In addition to high

brightness, another main advantage for Schottky emission source is that the current is very stable, which is because the tip is heated to nearly 2000°C and any contaminant would be burned off before it adsorb to the tip.

### 1.2.2.3 Cold Field Emission Source

This type is the truly field emission (tunneling) source. Electrons "tunnel out" from a tungsten wire because of the high field (~$10^8$V/cm) obtained by using a sharp tip (100 nm) and a high voltage (3-4kV). The emission current is called "cold" due to temperature independent (pure tunneling current, and operate at room temperature). Because it is cold, contaminates of gas molecule build up quickly, decreasing tunneling current with time, and causing high noise because the gas molecules adsorb and desorb from the tip randomly. It needs ultra-high vacuum (UHV), but gives long life and high performance. The benefit of cold field emission sources is extremely high brightness (~$10^9$ A/cm$^2$/rad) and a low energy dispersion (0.2-0.5 eV) of the emitted electrons. In addition to high current noise, cold field emission source has a lower attainable current than Schottky emission, with 10 $\mu$A being typical for commercial SEM. [15]

### 1.2.3 Limitations on Electron Beam Spot Size

The ideal ultimate electron spot size is given by [19]:

$$d_0 = \frac{d_v}{M}$$

***Where:*** $d_v$ is virtual source diameter and M (>1) is demagnification by the lenses.

Various aberrations of the electron optics lead to enlargement and distortion of the beam spot. Spherical and chromatic aberrations are the most significant for electron beam microscopy and lithography [20]

Spherical aberrations is due to that electrons passing through the outer zones of an electron lens have a shorter focal length. The final minimum beam diameter size limited by spherical aberrations is given by:

$$d_s = 0.5\ C_s \alpha^3$$

***Where:*** $C_s$ is the spherical aberration coefficient. For a well-designed magnetic lens, the spherical aberration coefficient is roughly equal to the lens focal length *f*. [21]

The chromatic aberration is due to the spread of electron energy (in eV). Obviously higher energy electrons are more difficult to focus by electron lens, thus they have farther focal points than lower energy electrons. The final minimum beam diameter size limited by chromatic aberration is given by:

$$d_c = C_c \frac{\delta V}{V} \alpha$$

***Where***: V is the accelerating potential and $C_c$ is the coefficient of chromatic aberration, which is approximately equal to the focal length of the lens for a well-designed lens.

In addition to the aberrations of lenses, the electron diffraction (as electrons are wave) lead to a minimum beam spot size of:

$$d_f = 0.61\frac{\lambda}{\alpha}$$

***Where:*** $\alpha$ ($\approx \sin\alpha$) is numerical aperture of the electron objective lens.

The de Broglie wavelength of electrons is given by:

$$\lambda = \left(\frac{h^2}{2mE}\right)^{\frac{1}{2}}$$

which is 0.008 nm for electron energy 25 keV and 0.0066 nm for electron energy 35 keV. With a typical value 2.5 mrad of $\alpha$, $d_f$ is about 3.1 nm for electron energy 25 keV and 2.6 nm for electron energy 35 keV.

The final beam spot size ($d_i$) is estimated by adding all the factors in quadrature:

$$d_i^2 = d_o^2 + d_s^2 + d_c^2$$

The beam diameter can be controlled through adjusting the beam current, accelerating voltage, and lens-to-sample spacing.[22] High-resolution electron beam lithography utilizes the highest accelerating voltage, lowest beam current, and smallest lens-to sample spacing. As an example, the Raith 150$^{TWO}$ for the nanofabrication work presented in this thesis features a tungsten filament Schottky emission gun, a maximum stable accelerating potential of 30 kV, and typical working distance of 10 mm (smaller working distance gives smaller beam spot size, but with higher risk of sample hitting the electron column).

### 1.2.4 Electron Scattering and Proximity Effect

The scattering of energetic electrons by the resist and the substrate is either elastic or inelastic, which leads to the exposed region being larger than the beam size. [23] The inelastic scattering of high-energy electrons through the resist can produce secondary electrons with energies ~10-50 eV. The scattered electrons are divided into two groups: one scattered through angles less than 90° and another scattered through angles greater than 90°. [15] The two groups of scattered electrons are called forward and backscattered electrons, respectively. Here the larger deflection angle scattering is with the nuclei and is elastic due to the mass mismatch between electron and the nuclei.

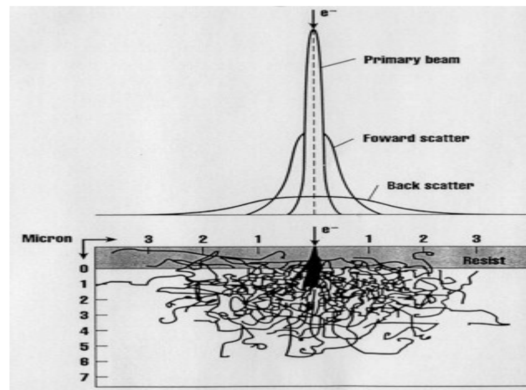

Figure 1-5: Interaction of electrons (forward and backward scattered) with resist-coated wafer [24]

Backscattered electrons result in the additional exposure of the resist to the primary beam exposure as shown in Figure 1-5. This is called the electron beam lithography proximity effect. [18]

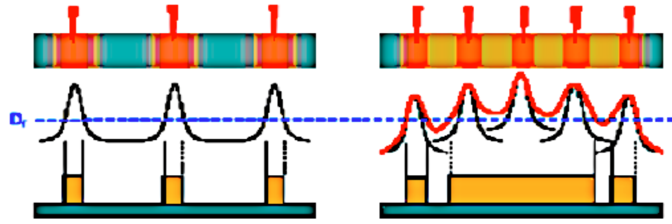

Figure 1-6: Patterns created by normal and additional exposure. [18]

The impact of scattered electrons is described by the double-Gaussian model [25]

$$exposure(r) = \frac{1}{\pi(1+\eta)}\left[\frac{1}{\beta_f^2}\exp\left(\frac{-r^2}{\beta_f^2}\right) + \frac{\eta}{\beta_b^2}\exp\left(\frac{-r^2}{\beta_b^2}\right)\right]$$

***Where:***

r is the radial distance from the beam position;

$ß_f$ is the forward scattered electron range (finite incident beam diameters are also modeled in $ß_f$);

$\eta$ is the ratio of integrated exposure from backscattered electrons relative to forward scattered electrons; and $ß_b$ is the backscattered electron range.

Therefore, the parameters for the double-Gaussian model are based on the incident beam energy, spot size, and the resist and substrate materials. [15] However, the exposure distribution is more precisely estimated by a double Gaussian plus an additional exponential term that exist if the desired patterns are on the order of 0.1 $\mu$m[26]

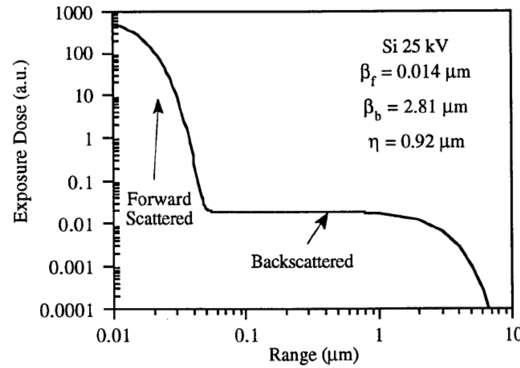


Figure 1-7: Double Gaussian model describing the scattering of electrons from a finite size source [26]

Figure 1-7 shows the double Gaussian model for 25 keV electron energy on silicon. [26] The actual exposure distribution is created by convoluting the point exposure response with the desired exposure pattern, and the areas not directly exposed by the incident beam are instead exposed by scattered electrons as a result of the influence of the proximity effect.[15]

To minimize the effect of proximity exposure, one way is to carry out the exposure on a resist coated on a membrane that is transparent to electrons (thus no backscattering). The proximity effect can also be compensated to a certain degree by Mont Carlo simulation and according dose adjustment. Certainly, proximity effect is less significant when the pattern is sparse, or when the pattern area is less than the range of backscattered electron.

### 1.2.5 EBL Resists

There are two types of EBL resist: positive and negative. Table 1-3 listed the popular e-beam resists and their properties.[27]

In positive resist, exposure to electrons result in rupture of the main and side polymer chains. The exposed area is thus easily soluble in its developer. The most popular positive tone e-beam resist is polymethylmethacrylate (PMMA) and ZEP-520. [28, 29, 30] The wide usage of PMMA for EBL is due to its general availability to provide high resolution with low cost and ease of process. The ZEP-520 (positive-tone, Zeon Corp.) is

the second most popular EBL resist. ZEP can achieve similar resolution to PMMA, and it offers higher sensitivity and etching resistance (see Figure 1-8). [31]

In negative resist, the areas exposed to electrons are cross-linked, thereby becoming less soluble in developers. Polystyrene (PS) is a simple negative resist, whose chemical structure is shown in Figure 1-9. PS is an appropriate resist for high resolution EBL.[32] Other negative resists include ma-N 2401 (Microresist Technology), SU-8 (Microchem Corp.), and mr-L 6000 (Microresist Technology).[33] The chemically amplified resists, SU-8 and mr-L 6000 provide higher sensitivity yet low contrast and resolution. [34] In addition, a non-polymer negative resist, calixarene, offers a very high resolution. The sensitivity of calixarene is 7000 $\mu C/cm^2$, which is significantly lower than that of PMMA. Calixarene has a contrast of about 1.6 with a developer of xylene. 12 nm diameter dots with a 25 nm pitch have been produced using calixarene. In addition, calixarene resists have a high resistance to plasma etching.

Common EBL resists with their properties and uses

| *Resist* | *Supplier* | *Tone* | *Sensitivity ($\mu C/cm^2$) at 100kV* | *Developer(s)* | *Characteristics* |
|---|---|---|---|---|---|
| PMMA (high molecular weight) | Microchem | Positive | 900 | Cellosolve Methanol 3:7 or MIBK:IPA1:3 or IPA:Water (conc. varies) | High resolution, single layer or top of Hi/Lo bilayer, liftoff |
| PMMA (low molecular weight) | Microchem | Positive | 800 | Cellosolve Methanol 3:7 or MIBK:IPA1:3 or IPA:Water (conc. varies) | High resolution, bottom of Hi/Lo bilayer, liftoff |
| Copolymer (MMA/MAA) | Microchem | Positive | 300 | Same as above | Large undercut profile for liftoff when used as bottom layer with PMMA on top |
| Zep520 | Zeon Chemicals | Positive | 300 | Hexyl Acetate, n-Amyl Acetate, or Xylenes | High resolution, good etch resistance |
| Zep7000 | Zeon Chemicals | Positive | 80 | 3-Pentanone Diethyl Malonate | Fast, good for making masks |
| NEB31 | Sumika Materials | Negative | 80 | 0.26N TMAH | Fast, chemically amplified resist |
| HSQ | Dow Corning | Negative | 1000 | 0.26N TMAH | High resolution, good etch resistance, flowable oxide |
| Calixarene | Synthesized | Negative | 10 000 or higher | Xylenes, IPA, MIBK | High resolution, good etch resistance |

Table 1-3: Popular e-beam resists and their properties [13]

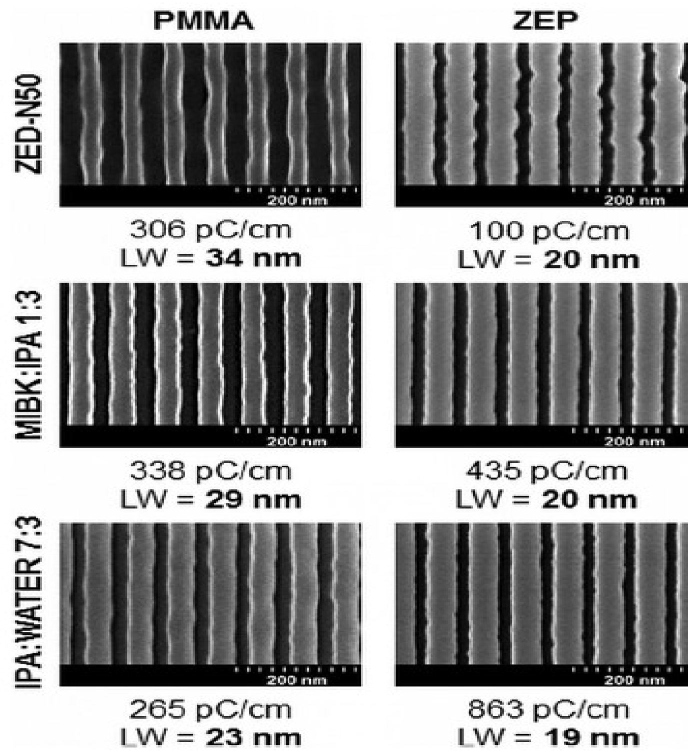


Figure 1-8: SEM images of 35 nm half-pitch PMMA and ZEP gratings exposed with 10 keV electrons and developed in ZED-N50, MIBK:IPA 1:3, and IPA: water 7:3 developers. The doses and minimum gap-widths achieved for each combination are noted. [31]

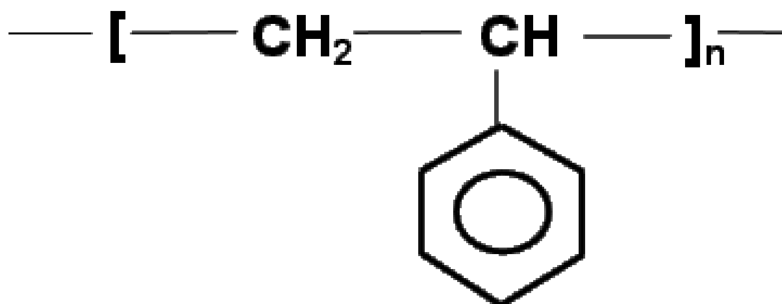


Figure 1-9: Chemical formula for polystyrene

As an example to illustrate the EBL process, we fabricated 300 nm period pillar array using ZEP, which is used to make a nanoimprint mold. In the experiment, we diluted ZEP 520A with anisole to give a 160nm film by spin-coating at 3000 revolution

per min (rpm) on a silicon wafer. The film was baked on a hotplate at 120$^{o}$C for 60min. After exposure at 20kev using Raith $^{Two}$ electron beam lithography system, the resist was developed in amyl acetate for 1 min at room temperature followed by rinsing in 2-popanol. Then the developed pattern was coated with a Cr film, followed by lift off by anisole for 40 min and then RIE 1 min. The result after exposure and liftoff is shown in Figures 1-10, 1-11, respectively.

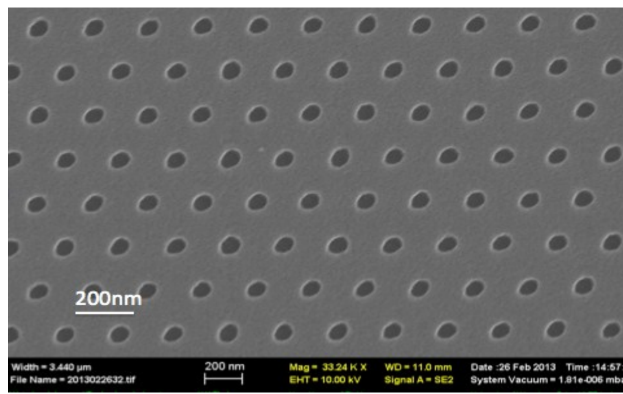


Figure 1-10: SEM image of 300nm period hole array exposed in ZEP resist

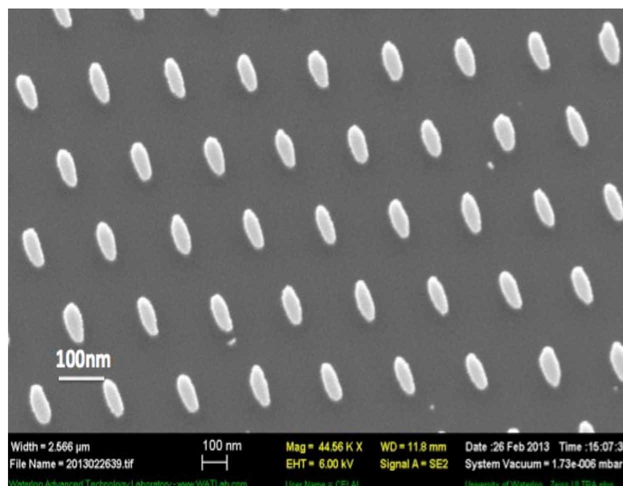


Figure 1-11: SEM image of 300nm period pillar array after liftoff and RIE

# CHAPTER 2: Dry thermal development of negative electron beam resists polystyrene (PS).

## 2.1 Introduction

In electron beam lithography, the exposed resist is typically developed using a solvent or aqueous developer. Potential issues with liquid developer include resist swelling, pattern detachment due to poor adhesion to the substrate, and resist pattern deformation and collapse due to capillary force during developer drying. To reduce pattern collapse due to capillary force, supercritical drying using $CO_2$ or fluoro-Compounds (e.g. $SF_6$ and $C_2HF_5$) can be employed. [35,36] However, pattern collapse still occurs, presumably due to the very high pressure of several MPa during the supercritical drying process. [37] Another way to minimize pattern collapse is by using sublimation of tert-butyl alcohol, whose melting temperature is slightly above room temperature. [38] One drawback of sublimation drying is that contaminant is left behind on the resist pattern when the solvent is vaporized. Therefore, dry development is still very desirable for some processes.

Auzelyte et al. recently demonstrated thermal development of a calixarene resist at 250-400oC, and achieved smooth line array patterns with 25 nm half-pitch. [39] As a small molecular resist, calixarene is a good candidate for thermal development. Polymer or co-polymer resists such as PMMA and ZEP-520A were also studied for dry thermal development, although without the pattern clearance that makes subsequently dry etching of the thick residual layer necessary. [40] Another approach of dry development is laser ablation, which was recently demonstrated for calixarene resist. [41] This method has made use of increased absorption thus ablation to 532 nm laser light when the calixarene resist was exposed to electron beam, hence calixarene changed its tone to positive when it was developed using laser ablation. One obvious limitation of this dry development approach is its extremely low throughput that is determined by the laser spot size (order 1 μm) and development time (order 1 sec).

Here it is shown that dry development can be realized using a simple electron beam resist polystyrene (PS), which has demonstrated ultra-dense patterning using low molecular

weight of 2 kg/mol, or ultra-high sensitivity lithography using high molecular weight of 900 kg/mol.[34, 42] Another advantage of this simple resist is its low cost, practically unlimited shelf life, and high drying etching resistance compared to PMMA. The dry development is possible because exposed thus cross-linked PS evaporates due to thermal decomposition at a slower rate than unexposed PS; therefore, the resist maintains its negative tone like regular solvent development.

**2.2 Experimental Details**

Polystyrene powder with molecular weights of 1.2 kg/mol (broad molecular weight distribution) and 2 kg/mol (narrow distribution with polydispersity 1.10) was dissolved in chlorobenzene. Here polystyrene with relatively low molecular weight was selected because it is more volatile than high molecular weight polystyrene at elevated temperatures for thermal development. The film thickness depends on the polystyrene concentration in the solvent and spin coating speed, ranging from 30 nm for 1.2 wt/vol% to 260 nm for 10 wt/vol concentrations. The film was baked at 60$^{o}$C for roughly half an hour on a hotplate. Though typical polymer film can be baked at temperatures much higher than its glass transition temperature (e.g. PMMA is usually baked at 180$^{o}$C), the thin polystyrene film having low molecular weight was not stable at baking temperatures above 80$^{o}$C, and thus we choose this very low baking temperature.

Electron beam lithography was performed at 20 keV and 5 keV using a LEO 1530 field emission SEM that is equipped with Nabity nanometer pattern generation system (NPGS) and a Raith 150$^{TWO}$ e-beam lithography system. The pattern contains arrays of large squares with a side length of 5 μm with exponentially varying doses that were used to obtain the contrast curve, and arrays of dense periodic lines that were used to determine the achievable resolution. The lines were exposed by single-pass exposure with a step size of 12 nm. After the exposure, the samples were developed thermally on a hotplate at 200$^{o}$C to 350$^{o}$C for 0.5-5.5 hours. Some samples were first developed using regular solvent developers (xylene for 30-72 sec, followed by rinsing with 2-propanol), then thermally developed in order to find out the development rate (nm/sec). After development, the contrast curves were obtained by AFM measurement, and high resolution images of the exposed pattern were acquired using LEO 1530 SEM.

## 2.3 Results and Discussion

The exposed pattern consisting of micro-scale squares appeared at development temperatures as low as 200°C. However, low temperature development led to poor contrast curve, as shown in Figure 2-1(a) for 1.2 kg/mol polystyrene developed at 250°C for 120 min. It is not possible to derive a meaningful resist contrast from this curve, although clearly the contrast is very low. The low contrast is not a result of the resist's broad molecular weight distribution, as it has been shown that the polydispersity (defined as Mw/Mn, the ratio of weight averaged molecular weight and number averaged molecular weight) had an insignificant effect on polystyrene's exposure properties.[43] The resist sensitivity, defined as dose for 50% remaining thickness, was approximately 3000 $\mu C/cm^2$, which is close to wet solvent development.

The low contrast makes the resist suitable only for grayscale lithography for which low contrast offers a broad process window and high reproducibility.[44, 45] Figure 2-1(b) shows the contrast curve for 2 kg/mol polystyrene developed at a high temperature of350°C for 30 min, which gives a moderately high contrast (defined as $\gamma=[\log\{D_{100}/D_0\}]^{-1}$) of 3.2, but a very low sensitivity ($D_{50}$, dose for 50% remaining thickness) of 16 $mC/cm^2$. The sensitivity can be greatly increased by using low voltage exposure such as 2 keV, because resist sensitivity (dose) is proportional to electron energy according to Bethe equation for electron energy loss ($E_{loss}$) in the resist: $E_{loss} \propto 1/E \cdot \log(\alpha E)$ with $\alpha$ being a constant.[46, 47] It should be noted that this temperature is close to the polystyrene decomposition temperature of approximately 650K (377°C), thus some degree of degradation is expected during the thermal development.

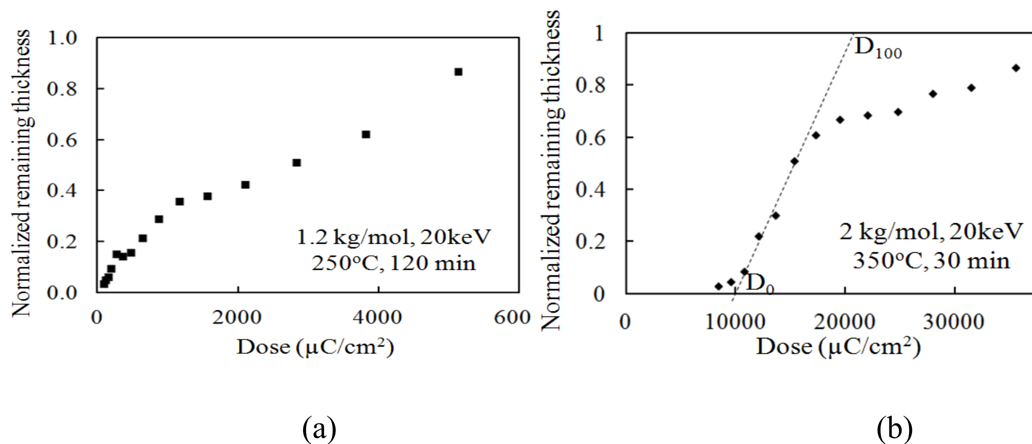


(a) (b)

Figure 2-1: Contrast curves exposed at 20 keV for (a) 1.2 kg/mol polystyrene thermally developed at 250°C for 120 min; and (b) 2 kg/mol polystyrene developed at 350°C for 30min.

To study the high-resolution capability of the thermally developed polystyrene resist, dense periodic array of lines were exposed. As shown in Figure 2-2 and expected from the resist contrast, reasonably high resolution of 30 nm half-pitch was achieved for thermal development at 350°C for 30 min. However, the obtained resolution is still much lower than polystyrene with the same molecular weight developed using a solvent, which has demonstrated 10 nm half-pitch patterning. [34] Due to its low sensitivity, the line dose to define the arrays was a very high 200 nC/cm, which is roughly 200 times that of PMMA at the same exposure voltage of 20 kV.

It is known that for regular solvent development, the development process proceeds from the resist surface towards the bottom, but not at a constant dissolution rate. For positive tone resist the kinetic diffusion-driven process predicts a reduced rate dz/dt as z increases (here t is the time of dissolution and z is depth reached at time t). [48] To investigate the thermal development process, the exposed pattern was first developed by using a solvent xylene to fully dissolve the unexposed polystyrene and partially dissolve the exposed one, thus creating an array of square pattern with different heights.

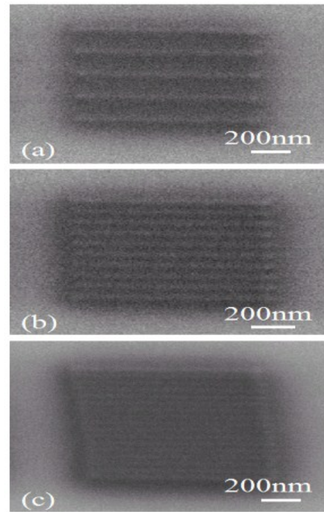


Figure 2-2: Dense periodic line arrays exposed at 20 keV and 96 pA beam current in 2 kg/mol polystyrene thermally developed at 350$^o$C for 30min. (a) 200 nm pitch, 50 nm line-dose; (b) 100 nm pitch; and (c) 60 nm pitch. Line dose was 200 nC/cm.

Next, thermal development was used to obtain the vaporization rate. Figure 2-3 shows the contrast curves for solvent development, solvent plus thermal development, as well as the absolute and relative thickness change (vaporization rate equal to thickness change divided by thermal development time). It is interesting to note that there exists a maximum thickness change, which corresponds to a large remaining thickness after wet development yet only a moderate exposure dose. Therefore, the development process cannot be a purely surface process for which monotonically decreasing thickness change versus exposure dose is expected since higher dose renders the resist more cross-linked thus less volatile. This implies that the less cross-linked molecules are mobile at the high development temperature and can move to the surface and vaporize. The decreased dissolution rate for thinner resist thickness is also expected for solvent development, but due to a different mechanism (kinetic diffusion of the solvent molecules into the resist). In addition, the dependence of vaporization rate on remaining thickness for thermal development is more pronounced than solvent development. Nonetheless, the relative thickness change, defined as the ratio of absolute thickness change and average thickness before and after thermal development, decreases monotonically with exposure dose, which is expected since higher dose renders the resist less volatile at elevated temperature.

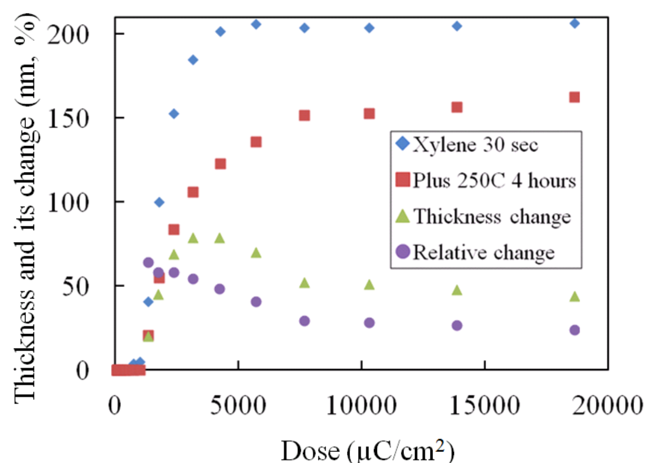


Figure 2-3: Contrast curves for 1.2kg/mol polystyrene exposed at 5 keV and developed first in xylene for 30 sec (diamond), and then thermally at 250$^{o}$C for 4 hours (square). The absolute (triangle) and relative (circle) thickness change due to thermal development are also shown for doses that led to non-zero remaining thickness after thermal development. The relative change is defined as the ratio of absolute thickness change and average thickness before and after thermal development.

## 2.4 Conclusion

We have demonstrated dry thermal development of negative resist polystyrene. When developed on a hotplate at 350$^{o}$C for 30 min, polystyrene showed reasonable high contrast and resolution, but very low sensitivity. Resist sensitivity was greatly improved at lower development temperatures, though at the cost of reduced contrast. In addition, by developing the exposed pattern first using a solvent then thermally, we observed the thickness reduction due to thermal development was larger for thicker patterns, implying the thermal development process is not just a surface process and the more volatile chains below the top surface can diffuse to the surface and get evaporated. However, as expected, the relative thickness change decreased monotonically with increased exposure dose.

# CHAPTER 3: Polycarbonate electron beam resist using solvent developer

## 3.1 Introduction

Electron beam lithography (EBL) [49], focused ion beam (FIB) lithography [50], and nanoimprint lithography (NIL) [51] are currently the three most widely employed nanolithography techniques. Amongst them, EBL is undoubtedly the most popular for R&D. Sensitivity and contrast are the two most important resist properties. Higher sensitivity is always desirable since it allows fast writing. As for contrast, high contrast is usually preferable since it offers high resolution patterning. It has been proven that resists having high sensitivity tend to have low contrast, and vice versa. [52] For instance, regarding resist development temperature (keeping other experimental conditions identical), cold development of positive resists such as PMMA and ZEP enhances contrast but lowers sensitivity.[52] Regarding resist molecular weight, higher molecular weight (Mw) polystyrene (negative chain cross-linking resist) offers higher sensitivity than lower Mw polystyrene, but gives lower contrast and thus lower resolution.[34, 42] Other important resist properties include chemical inertness, thermal stability, and dry etch resistance. PMMA (the most popular positive resist) is far from ideal in those aspects. The arguably second most popular positive resist, ZEP, offers much higher (roughly three times) dry etch resistance than PMMA due to the stable phenyl group in its structure. Polycarbonate (PC), which is the focus of the current study, offers significantly higher chemical and thermal stability than both PMMA and ZEP, and its dry etch resistance (to oxygen plasma RIE), though not as high as ZEP resist, is approximately twice that of PMMA.

Owing to its chemical and thermal stability, PC has been widely used for filtration and nano-wire or nano-tube synthesis applications with the through-film hole created by the ion-track etch process. [53, 54, 55, 56, 57] As such, PC is a sort of ion beam resist. Recently it has been demonstrated that PC can also be used as an electron beam resist with hot

aqueous NaOH as developer and gold film as sub-layer. [58] A serious concern is the potential attack of the substrate material by hot NaOH solution and the weak adhesion of PC to typical substrate materials such as silicon, which lead to film detachment during development. It is therefore desirable to replace the hot basic development with room temperature solvent development. In this study we show that PC can be developed using solvent, but with very low contrast. Thus, PC is a suitable resist for grayscale lithography.

Grayscale lithography is commonly used to generate 3D structures such as arbitrarily sloped sidewall, multi-level zone plate/Fresnel lens, and micro-lens with hemispherical shape. [59, 60] The 3D features are achieved in a single resist layer by positive or negative tone electron beam resist. While in principle high resolution resist with high contrast such as PMMA can be used for grayscale lithography, this is not desirable because a slight variation of exposure dose (or development temperature) would result in a considerable change in resist height after development, thereby leading to a very narrow process window. In contrast, low contrast resist such as polycarbonate developed using a solvent offers a broad process window for reproducible results.

**3.2 Experimental**

To dissolve PC, we tested many different solvents including dioxane, 1, 2, 3 - trichloropropane, tetrahydrofuran, dichlorobenzene, and cyclopentanone. However, unlike PMMA or ZEP resist, most solvents cannot easily dissolve PC to form a homogeneous transparent solution. It was found that dissolution could be facilitated by using ultrasonic agitation for several hours. Cyclopentanone was identified as the best solvent that can dissolve PC pellets (2.5 wt/vol % that gave 95 nm film thickness by spin-coating at 2000 rpm) in ~10 hours, or in ~4 hours with ultrasonic agitation. For higher concentration such as 10 wt/vol % that gave 1200 nm film thickness, ultrasonic agitation was essential for the dissolution (not completely dissolving even after more than three days without ultrasonic agitation).

It is natural to first try cyclopentanone as developer. Since cyclopentanone quickly dissolves unexposed PC film, it must be diluted with a non-solvent in order to act as a reasonably good developer. We diluted cyclopentanone with 2-propanol (IPA) gradually until the mixture was found to not attack the unexposed PC film significantly within three

minutes of soaking. This is obtained with cyclopentanone : IPA=1:3. Using a similar screening procedure, we also studied other solvent developers including xylene, pentyl acetate (both are developers for ZEP), methyl isobutyl ketone (MIBK, developer for PMMA), and propylene glycol monomethyl ether acetate (PGMEA, developer for SU-8). All of those solvent developers, when properly diluted with IPA, can act as developer for PC with performance similar to diluted cyclopentanone.

We dissolved 60 kg/mol (polydispersity unknown) bisphenol A polycarbonate (Scientific Polymer Products Inc.) in cyclopentanone. We selected this molecular weight mainly due to its availability from the supplier. Unlike negative chain cross-linking resist such as polystyrene, for positive chain scission resist it is expected that molecular weight would not greatly affect the exposure properties, nor is its distribution (i.e. polydispersity).[61, 43] The film was then baked on a hotplate at 140$^{o}$C for 2 min. After exposure at 20 keV using Raith 150$^{TWO}$ electron beam lithography system, the resist was developed for 0.5 - 1 min at room temperature followed by IPA rinsing and nitrogen drying.

To attain the contrast curves, the pattern containing 5 × 5 array of squares each 5 µm × 5 µm was exposed with exponentially increasing doses. The wide range of exposure doses enabled detailed study of PC resist's performance. After development, the pattern depth was measured using atomic force microscope (AFM) to generate the contrast curves. To study PC's high resolution capability, single-pass lines at various doses were also exposed using the same condition and the lines were examined using SEM after development.

### 3.3 Result and discussion

Figure 3-1 shows the contrast curve of polycarbonate exposed at 20 keV and developed using cyclopentanone : IPA = 1:3 for 1 min at room temperature. Figure 1b is the contrast curve with dose in log-scale in order to better present the curve for low doses. The dose for clearance ($D_{100}$) is approximately 2000 µC/cm$^2$; that for 50% remaining thickness ($D_{50}$) is approximately 180 µC/cm$^2$; and $D_0$ is 25 µC/cm$^2$. This leads to a contrast (defined as $\gamma=[\log_{10}(D_{100}/D_0)]^{-1}$) of 0.53, which is a very low value. Thus, solvent-developed PC is not suitable for defining high resolution dense pattern. Figure 3-

1c is the contrast curve with dose in linear scale. It is not possible to derive a meaningful contrast as the $D_0$ value would approach 0 μC/cm$^2$. Figure 3-1c indicates that the remaining resist thickness drops very fast with increasing doses when the dose is low (<300 μC/cm$^2$), but then the residual layer becomes less easy to dissolve as the dose increases.

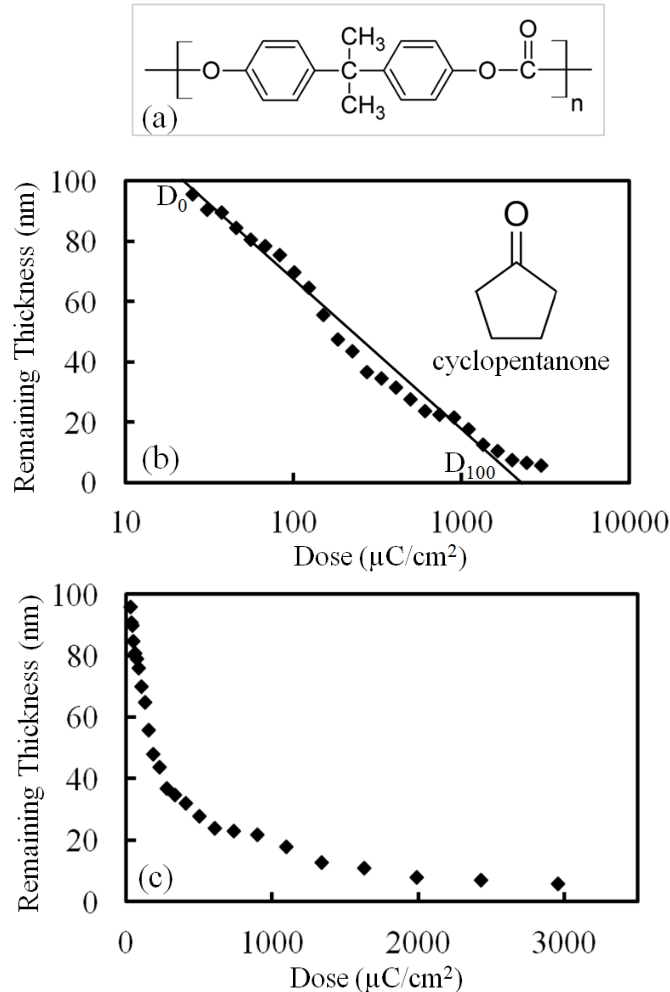


Figure 3-1: (a) Chemical structure of bisphenol A polycarbonate; (b) Contrast curve for polycarbonate exposed at 20 keV and developed by cyclopentanone : IPA = 1:3 for 1 min, with the dose in log-scale; and (c) Same as (b) but with dose in linear-scale.

The contrast curves for PC developed using xylene (p-, m-, o- mixed) and pentyl acetate are shown in Figure 3-2 and Figure 3-3, respectively. Both solvents were diluted with IPA at 1:3 volume ratio. When using xylene as developer, the resist sensitivity ($D_{100}$) and contrast are 2360 μC/cm$^2$ and 0.84, respectively; and those for pentyl acetate, 2800 μC/cm$^2$ and 0.91, respectively. The contrast for both solvent developers is higher

than cyclopentanone, yet still much lower than typical high resolution resist. We also studied other solvent developers diluted with IPA at 1:3 ratio, such as PGMEA (developer for SU-8) and MIBK (developer for PMMA), and found that both can act as developer for PC with performance similar to the above solvent developers.

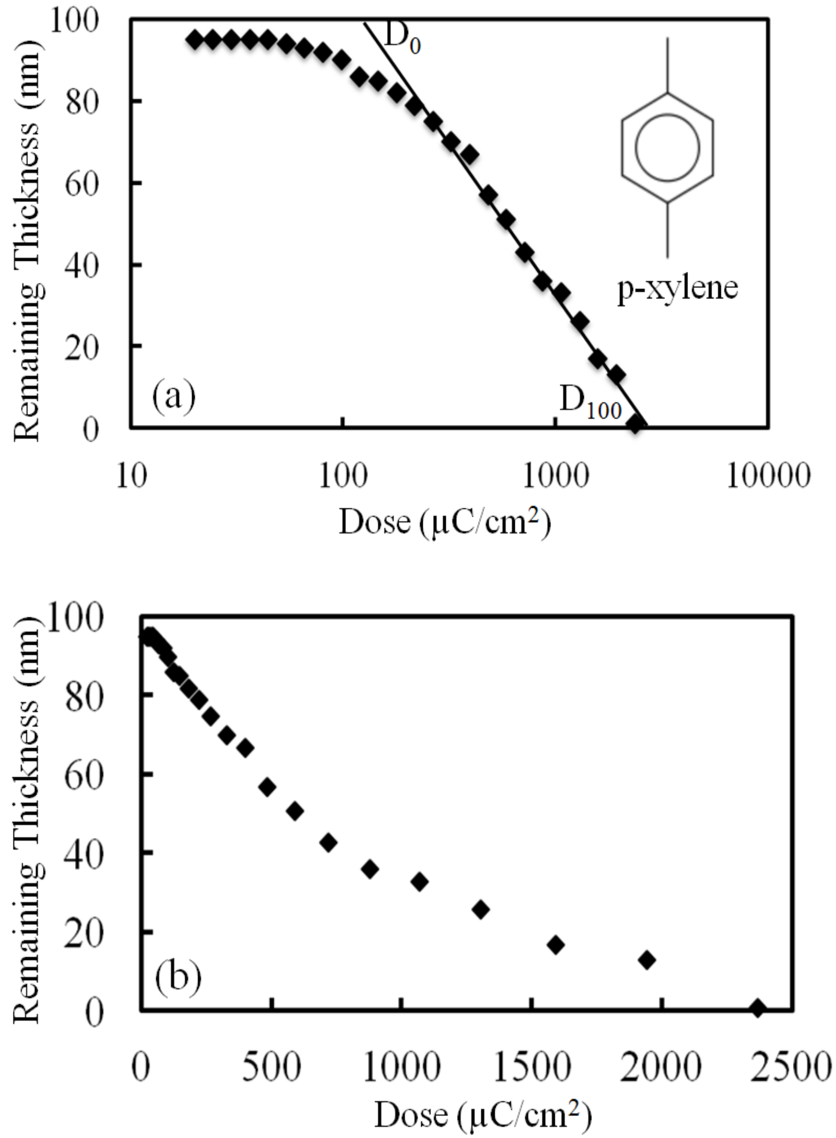


Figure 3-2: Contrast curve for polycarbonate exposed at 20 keV and developed by xylene: IPA = 1:3 for 1 min, with dose in log-scale (a) and linear-scale (b). The xylene is p-, m-, o- mixed.

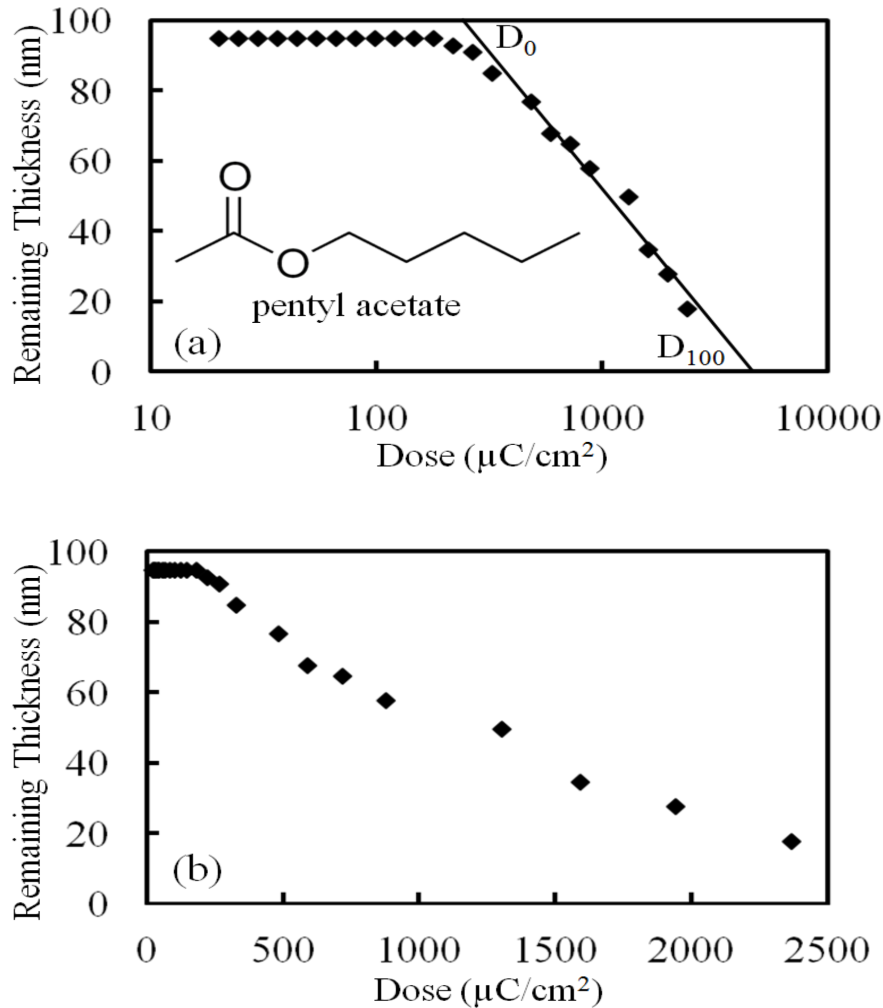


Figure 3-1: Contrast curve for polycarbonate exposed at 20 keV and developed by pentyl acetate : IPA = 1:3 for 0.5 min, with dose in log-scale (a) and linear-scale (b).

Although the low contrast suggests that PC is suitable for grayscale lithography but not for defining high resolution dense patterns, PC is able to pattern sparse high resolution features. In fact, SU-8, which is also a very low contrast resist, has demonstrated high resolution of 24 nm when exposed at 100 keV.[62] Figure 3-4 shows line array pattern with 1000 nm period exposed in PC at 20 keV and developed by diluted cyclopentanone, which gives a high resolution of 48 nm. This is possible when the pattern is sparse and/or the pattern area is significantly smaller than the range of backscattered electrons, such that the proximity effect is unimportant.

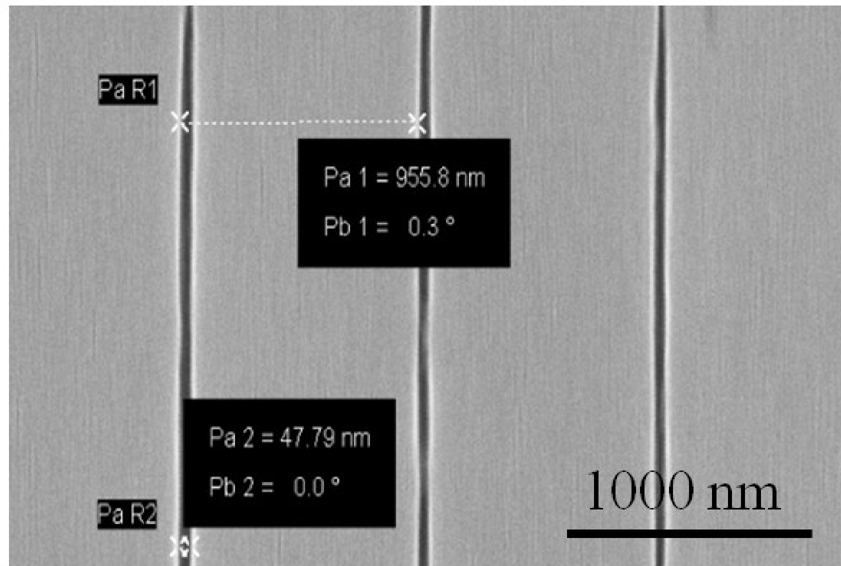


Figure 3-2: SEM image of line array pattern exposed in PC at 20 keV and developed by cyclopentanone (diluted with IPA at 1:3 volume ratio). The line width is close to 50 nm and array period is 1000 nm.

### 3.4 Summary

In this study, we investigated the possibility of using solvent as developer for polycarbonate electron beam resist, which is more desirable than the usual hot aqueous solution of NaOH developer. We found that actually many solvents (including cyclopentanone, MIBK, xylene, pentyl acetate, and PGMEA), when properly diluted by a non-solvent for polycarbonate (here IPA), can be used as developers for polycarbonate. All of the solvent developers we tested give a low contrast between 0.5 and 1.0, making polycarbonate a suitable resist for grayscale electron beam lithography. Despite its low contrast, polycarbonate can also be used for high resolution lithography when the pattern is not dense and/or the pattern area is much smaller than the range of backscattered electron (thus insignificant proximity effect); and we achieved sub-50 nm line-width definition for a line array with 1000 nm periodicity.

# CHAPTER 4: Metal nanostructure fabrication by electron beam lithography and *dry* liftoff

## 4.1 Introduction

Liftoff and direct etch are the two most popular pattern transfer processes. Figure 4.1 schematically showed the two processes, taking the fabrication of metal nanostructure as an example. In the direct etch process, first metal film and electron beam resist are coated on the substrate by physical vapor deposition and spin-coating, respectively. Then thin resist layer is exposed to electron beam lithography (EBL) and developed, to form the desired pattern in the resist layer. Finally the metal is etched by RIE with the resist as etching mask, followed by resist removal. In the liftoff process, electron beam resist is first coated on the substrate by spin-coating. Next, the resist is exposed to EBL, and developed to form the desired pattern in the resist layer. Then metal is coated onto the resist pattern by evaporation. Finally the resist is dissolved in a solvent or aqueous solution, and as a result, the metal on top of resist is lifted off when the resist underneath is dissolved.

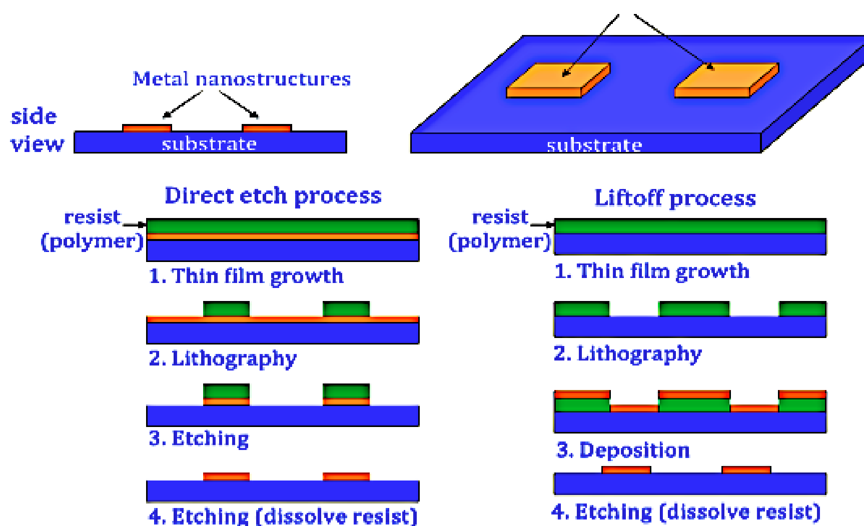

Figure 4-1: Schematic liftoff and direct etch method for pattern transfer, here transferring the polymer resist pattern into metal pattern.

Compared to direct etch, liftoff is more versatile since it can work for most metals, whereas very few metals can be etched by dry etching (e.g. Al, Ti, W, and Cr). However, for liftoff, the solvent or aqueous solution that dissolves the resist must not attack the substrate materials, which can be a conducting polymer for some applications. As a result, solvent-free liftoff or dry liftoff process is desirable.

**4.2 Dry Liftoff**

In dry liftoff, the patterned film coated with the metal is peeled off the substrate, rather than dissolved by a solvent. Obviously the adhesion of the resist to the substrate should not be too strong, as otherwise the film will be broken during the peel off process. Some materials such as polycarbonate have weak adhesion to the silicon substrate, thus it can be peeled off easily by using scotch tape. Other materials such as PMMA have strong adhesion to silicon wafer, thus the substrate surface must be modified with a surfactant which has a low surface energy (e.g. a self-assembled monolayer (SAM) of perfluorooctyltrichlorosilane (FOTS)) in order to reduce its surface energy such that the PMMA can be peeled off. However, the surface energy cannot be too low, as otherwise the resist solution will form droplets on the substrate surface, and thus a uniform resist film cannot be coated onto the substrate by spin-coating. In addition to surface energy and adhesion, another important factor is the resist cross-sectional profile.

An undercut profile is ideal for liftoff process. As seen in Figure 4.2, with such a profile, the metal on top of resist is not connected to the metal on the substrate. Otherwise, with a tapered (V-shaped) profile, the metal film on top of resist will be connected to the metal on the substrate through the metal coated on the sidewall (now that the sidewall is tapered). Therefore, it would be very difficult to obtain a clean lift off pattern.

Undercut profile
for liftoff

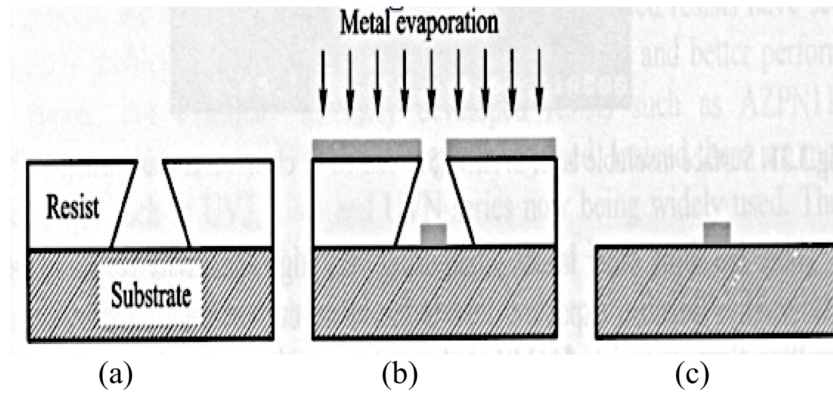


Figure 4-2: Metal lift-off process [11], (a) Ideal resists profile, (b) Deposition of metal, and (c) After lift-off

### 4.3 Dry Liftoff Using Polycarbonate (PC) Resist

#### 4.3.1 Reason for Using Polycarbonate

For dry liftoff, it is critical to control the interface energy between the resist film and the substrate. Too high interface energy leads to strong adhesion and makes peeling-off impossible, whereas too low substrate surface energy makes spin-coating difficult. For polycarbonate e-beam resist, [63] no substrate treatment is needed since it adheres poorly to bare silicon wafer. In fact, we have had difficulty to achieve a strong adhesion needed for EBL development using hot NaOH aqueous solution as developer. This fact encouraged us to try polycarbonate resist first for dry liftoff.

#### 4.3.2 Experimental Details

In the experiment, we dissolved 60 kg/mol bisphenol A polycarbonate in cyclopentanone to make a 4 wt/vol% solution that gave a 200 nm uniform film by spin-coating at 1200 rpm on a silicon wafer. The film was then baked on a hotplate at 120$^{o}$C for 5 min. After exposure at 20 keV using Raith 150$^{TWO}$ electron beam lithography system, the resist was developed in a 1:3 mixture of cyclopentanone and 2-propanol for 30 sec at room temperature followed by rinsing using 2-propanol. Finally we coated 10 nm Cr and peeled off the resist film using a polyimide tape.

### 4.3.3 Results and Discussion

As seen in Figure 4-3, the process worked but the pattern is not “clean” with very rough edges. This is obviously because of the tapered (V-shaped) profile of the polycarbonate resist pattern, which is in turn due to the low contrast of polycarbonate resist. During the peeling off, the metal film is broken, leading to rough edges. The thickness of the film on the sidewall depends on the taper angle θ (proportional to cosθ, equal to 0 when the sidewall is vertical), and should be <3 nm. However, the metal film seems to be torn off away from this thinner part of the film.

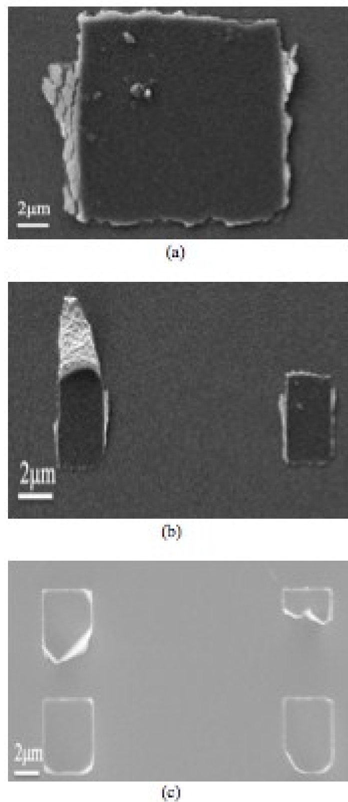


Figure 4-3: SEM image of a stack of PC on silicon wafer created by e-beam writing at 20 keV; using a 1:3 mixture of cyclopentanone and 2-propanol; and after dry lift off process; a) Zoom-in scan to show the edge; b) Zoom-in scan of two squares an array, c) Zoom-out scan of an array.

## 4.4 Dry Liftoff Using Bi-layer Polycarbonate and PMGI

### 4.4.1 Reason for Bi-layer

PC results in a tapered profile, which leads to difficulty in clean dry liftoff. Due to its low contrast, it is difficult to achieve an undercut profile using just single layer of polycarbonate (PC) resist. Thus we turned to a bi-layer resist structure in order to achieve the undercut profile. PMGI (polymethylglutarimide, SFG 2 S from MicroChem Corp.) is a very popular liftoff layer, so it is chosen for our purpose. Initial test showed that, as expected, PMGI didn't detach from the silicon wafer since it adheres strongly to silicon; instead PC detached from the PMGI layer. This is acceptable for dry liftoff since the metal on top of the resist layer is removed when PC is peeled off. We expected to achieve an undercut profile because PMGI is a more sensitive resistant than PC (PMGI is exposed during the exposure of PC). We designed the process steps as shown in Figure 4-4.

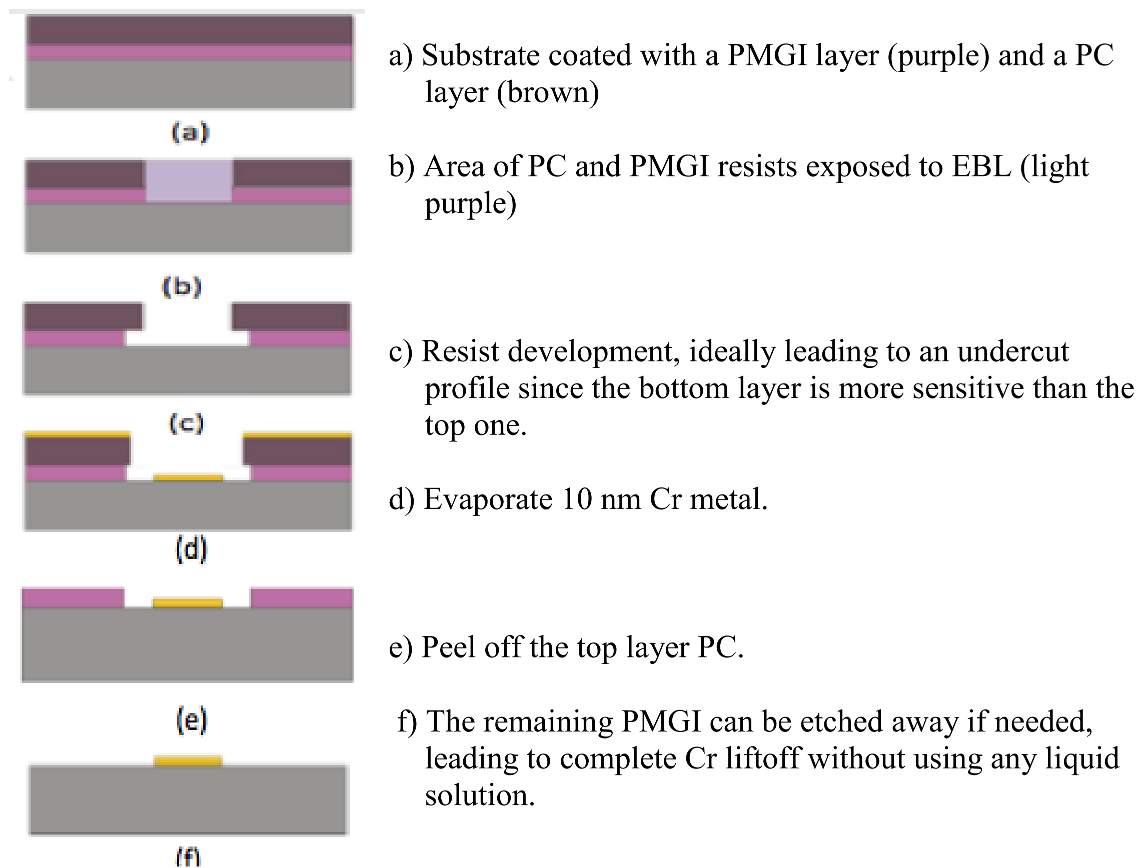


Figure 4-4: Process using PC/PMGI bi-layer resist for dry liftoff [64]

### 4.4.2 Experiment Details

In the experiment, the first layer PMGI gave a 60 nm thick uniform film by spin-coating at 2000 rpm on a silicon wafer. The film was then baked on a hotplate at 180$^{o}$C for 30 min. After that, we spun the second layer of PC film with a 4 wt/vol% solution to give a 200 nm uniform film by spin-coating at 1200 rpm on a silicon wafer. The film was then baked on a hotplate at 120$^{o}$C for 5 min. After exposure the development was conducted at room temperature for PC resist in a 1:3 mixture of cyclopentanone and 2-propanol for 1 min, followed by PMGI development in a 1:3 mixture of MIPK:IPA for 3 min. Finally 10 nm Cr was coated and lifted off using a polyimide tape.

### 4.4.3 Results and Discussion

As seen in Figure 4-5, the result after dry liftoff using this bi-layer resist is even worse than using single layer PC resist. After some test, we found out that the solvent cyclopentanone used for PC coating actually attacks the underneath PMGI film, thus there is no clear boundary between the two films as needed for an undercut profile. In addition, the developer (diluted cyclopentanone) for PC also develops fast the exposed PMGI area. Therefore, this method is proven not feasible for dry lift off process.

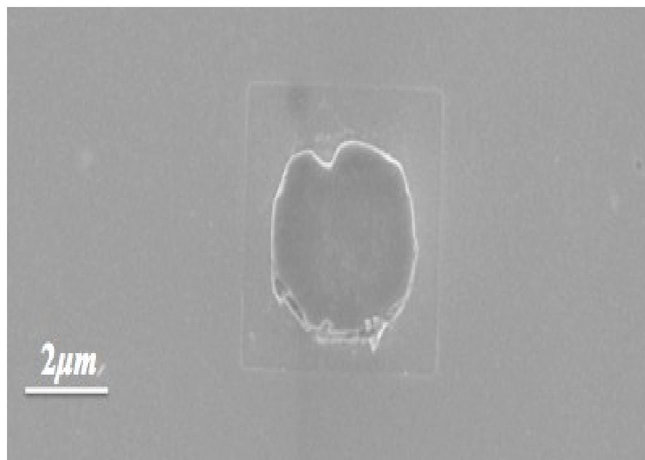


Figure 4-5: SEM image of 10 nm-thick Cr pattern fabricated by dry liftoff, with poorly defined square pattern.

### 4.5 Dry liftoff using PMMA resist

#### 4.5.1 Reason for Using PMMA

As mentioned above, polycarbonate is not suitable for high resolution dry liftoff since it has low contrast. Therefore we studied PMMA that is the most popular high resolution e-beam resist. As PMMA has strong adhesion to silicon substrate, surface treatment of the substrate is indispensible.

#### 4.5.2 Experiment Details

We first treated the silicon wafer with low surface energy SAM (self-assembled monolayer) of perfluorooctyltrichlorosilane (FOTS). We placed the wafer and a drop of FOTS inside a box (with no vacuum) and optimized the treatment time (30 min) so that the surface energy is suitable for both peeling-off and spin coating of PMMA dissolved in a non-polar solvent toluene (996 kg/mol PMMA, 3 wt/vol%, 560 nm-thick film at 2000rpm, film baked on hotplate at 120 $^{o}$C for 10 min). Here we cannot use the more popular solvent for PMMA, notably anisole and chlorobenzene, since they are both polar and thus don't "wet" the silicon substrate coated with the anti-adhesion SAM layer, leading to no film formation. Alternatively, for substrates not compatible with such anti-adhesion treatment, a low surface energy thin fluorocarbon film may be coated using CHF3, C4F8, or CF4/H2 plasma. After exposure at 20 keV using Raith$^{TWO}$ electron beam lithography system, the resist was developed in IPA: $H_2O$ =7:3 for 1 min due to its low swelling (the more popular developer, MIBK (methyl isobutyl ketone) : IPA = 1:3 swells the PMMA more than IPA:$H_2O$, thus it may peel off the resist now that its adhesion to the silane-treated substrate is low). Next, 10 nm Cr was coated by e-beam evaporation followed by dry liftoff using scotch tape to peel off the film (see Figure 4-6).

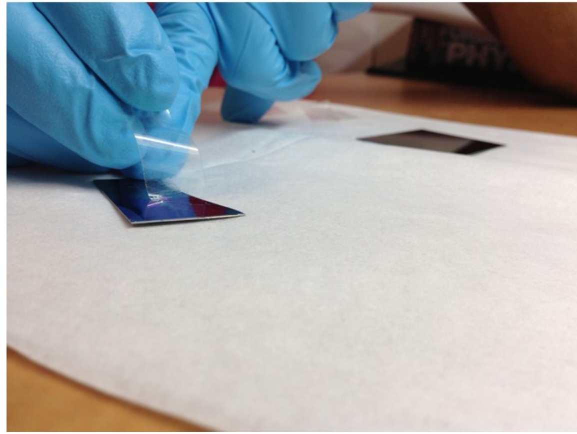

Figure 4-6: Photograph showing the peeling off process of the resist film using scotch tape

### 4.5.3 Results and Discussion

Figure 4-7 shows Cr patterns fabricated by electron beam lithography and dry liftoff. The substrate Si was etched by RIE in order to obtain higher image contrast. Line array with 56 nm line-width and large squares with doses increasing exponentially from lower left to upper right were obtained. The size increase for the squares exposed at higher doses is due to proximity effect. At very high doses, PMMA becomes a negative resist and the cross-linked area (the three squares at upper right) was not peeled off.

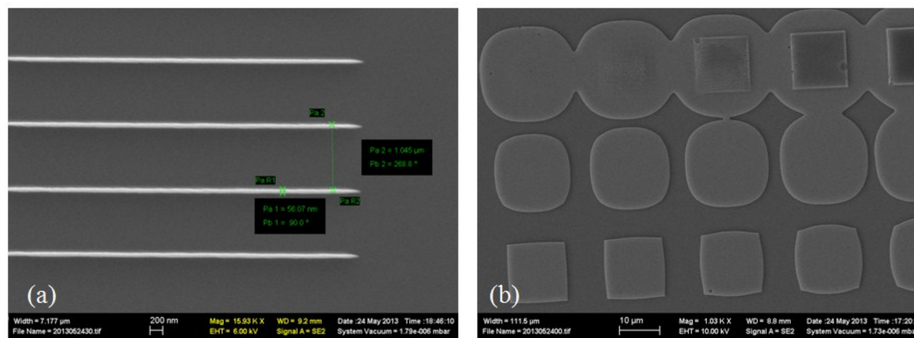


Figure 4-7: SEM images of Cr patterns fabricated by electron beam lithography and dry liftoff, (a) Line array with 56 nm line-width; and (b) Large squares having doses increasing exponentially from lower left to upper right.

### 4.5.4 Conclusion

Here we explored the potential of using dry liftoff to fabricate metal nanostructures. The liftoff is realized by mechanically peeling off the metal-coated resist film, rather than dissolving the underlying resist using a solvent as is the case for conventional liftoff process. Low resolution dry liftoff was achieved by using polycarbonate resist, whereas high resolution down to 50 nm was obtained by using PMMA resist coated on a low surface energy substrate.

# CHAPTER 5: Water soluble and developable electron beam resist PSS

## 5.1 Introduction

In electron beam lithography, exposed resist is typically developed in solvent such as PMMA resist in MIBK:IPA, or base solution such as HSQ resist in aqueous TMAH. For spin coating, the resist is usually dissolved in a strong solvent such as anisole. However, for some applications, such as nano-patterning on top of a semiconducting polymer or a regular polymer substrate like PMMA, solvent or the strong base solution may attack the substrate material. Here we showed that, poly (sodium 4-styrenesulfonate) (PSS), which is soluble in water due to its ionic nature, can be used as a negative electron beam resist developed in water. This is not surprising given that its chemical structure is similar to that of polystyrene, which is a popular negative tone electron beam resist. [65, 43] It is known that PEDOT: PSS (here PSS is an acid, rather than a salt) is one of the most popular conducting polymers used for solar cells as well as organic light-emitting diodes. [66] Its electrical properties might be altered favorably by electron beam exposure.

## 5.2 EBL of PSS Coated on Bare Silicon Wafer

In the experiment, we dissolved 70 kg/mol PSS (Sigma Aldrich) in DI water to make a 5 wt/vol% solution that gave a ~60 nm film by spin coating at 2000 rpm. The film was then baked on a hotplate at $90^oC$ for 5 min to drive off the water. Next, the resist was exposed at 20 keV using Raith $150^{TWO}$ electron beam lithography system. After that, the resist was developed in DI water for 10 sec at room temperature, and dried by $N_2$ gun.

However, we found that most exposed square patterns were peeled off, except those few that were exposed with high doses. This may be because of poor adhesion of PSS to silicon wafer and the fact that water can penetrate into the PSS film and swell it.

## 5.3 EBL of PSS Coated on PMMA/Si

In order to improve the adhesion, we coated PMMA on silicon wafer, onto which PSS was spun-coated. In the experiment, we spun coat PMMA at 5000 rpm to get a film of

245 nm. The film was baked on hotplate at 120$^{o}$C for 10min, and we dissolved 70 kg/mol PSS in DI water to make a 7 wt/vol% solution that gave a ~180 nm film by spin coating at 1200 rpm (see Figure 5-1). The film was then baked on a hotplate at 90$^{o}$C for 5 min to drive off the water. Afterwards, the resist was exposed at 20 keV using Raith 150$^{TWO}$ electron beam lithography system. Finally, the resist was developed in DI water for 10 sec at room temperature, and then rinsed it in IPA that has lower surface energy than water thus less peeling off.

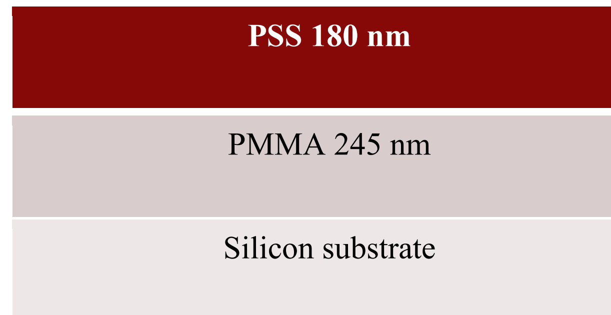


Figure 5-1: PSS on PMMA to solve the adhesion issue of PSS to silicon.

However, we found that the PMMA under-layer was attacked by IPA. This is because, even though in normal condition IPA doesn't attack PMMA, it will do so when PMMA is exposed and when there is water. In fact, a mixture of IPA and water at 7:3 ratio is a popular developer for PMMA, even though none of the two liquid will develop PMMA when used alone.

**5.4 EBL of PSS Coated on ARC/Si**

We spun coat PSS to make 180 nm film by spin coating at 1200 rpm on top of ~100nm ARC (anti-reflection coating, a commercial cross-linked polymer). The film was then baked on a hotplate at 90$^{o}$C for 5 min. Afterwards, the resist was exposed at 20 keV using Raith 150$^{TWO}$ electron beam lithography system. Finally, the resist was developed in DI water for 10 sec at room temperature, rinsed in IPA that has lower surface energy than water thus less peeling off, and dried by $N_2$ gun.

Figure 5-2 shows the contrast curve measured by AFM as well as the AFM images of the dose test pattern containing a 5 by 5 array of squares each 5 μm × 5 μm. The

sensitivity of PSS (defined as $D_{50}$) is approximately 2809 $\mu C/cm^2$. This is about one order lower than that of PMMA, but we expect much higher sensitivity for PSS with higher molecular weights such as 1000 kg/mol, if its exposure property is similar to polystyrene whose sensitivity ($\mu C/cm^2$) is inversely proportional to its molecular weight (kg/mol). The contrast (defined as $\gamma=[\log_{10}(D_{100}/D_0)]^{-1}$) is also a low value of 0.77. Thus PSS is not suitable for patterning dense and high-resolution structures. Nonetheless, feature size down to 50 nm was achieved for sparse patterns, as shown in Figure 5-3. SEM image displays the resolution capability of PSS line arrays with a period of 779 nm and line-width 50nm.

Moreover, since sodium PSS contains metal sodium, it is far more resistant to plasma etching than PMMA. For instance, its etching rate by oxygen plasma RIE was found to be only 1/17 that of PMMA ($O_2$ RIE condition: 20W, 20mTorr, 20sccm etch rate PSS 10nm/min, PMMA 174nm/min). For RIE using $CF_4$ gas (20sccm, 20mTorr, 100W), the etch rate selectivity is PSS:Si:PMMA = 0.73:1:2.54, that is, PSS is 3.5× more resistant to CF4 RIE than the popular electron beam resist PMMA. Even lower etching rate is possible if sodium in sodium PSS is replaced with another metal such as nickel.

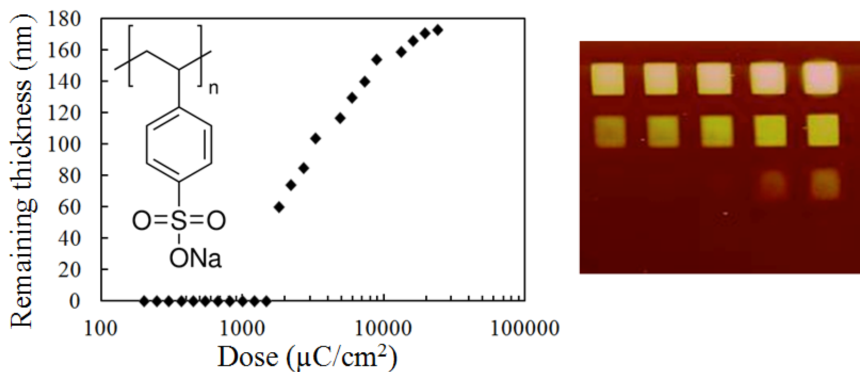


Figure 5-2: Contrast curve for sodium PSS exposed at 20keV and developed in DI water for 10 sec. The sensitivity ($D_{50}$) and contrast are derived as 2800 μC/cm2 and 0.8, respectively. Also shown are the chemical structure of the resist and AFM image of the large (5µm by 5µm) exposed square array used to generate the contrast curve.

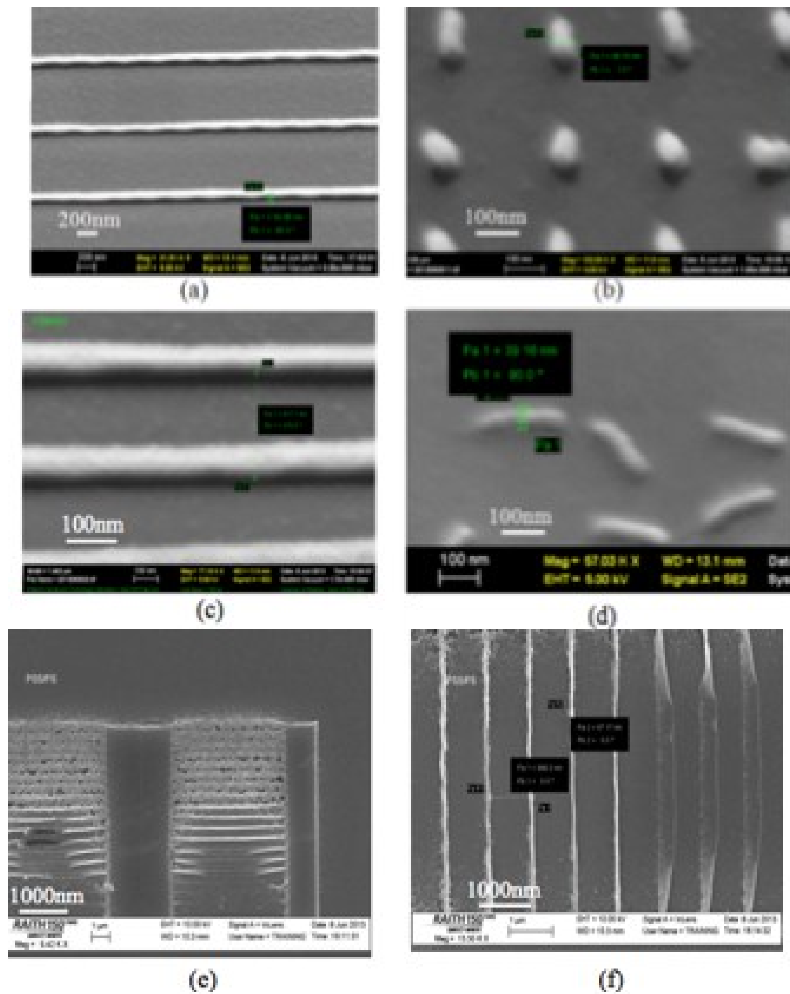


Figure 5-3: High resolution pattern in sodium PSS by electron beam lithography at 20 keV. (a, c) Line array with line-width ~50 nm and pitch 400 nm. Narrower lines were found collapsed. (b, d) Pillar array with diameter 40 nm or 60 nm and height close to 150 nm. Again the smaller pillars fell off cue to capillary force during developer drying. (e, f) Zoom out view of the line array exposed at different doses. Too low dose resulted in narrow lines that fell off; whereas too high dose resulted in merged lines (upper part in (e)) due to over-exposure.

### 5.5 Conclusion

To conclude, we proved that poly (sodium 4-styrenesulfonate) (sodium PSS), which is soluble in water due to its ionic nature, can be used as a negative electron beam resist developed in water. Sodium PSS is not appropriate for patterning dense and high resolution structures. Nevertheless, feature size down to 40 nm was achieved for sparse patterns.

# Chapter 6: Fabrication of membrane-supported gold nanostructure for x-ray imaging

## 6.1 Introduction

Previously Prof. Gu Xu's group from McMaster University has demonstrated novel x-ray imaging method using the "Borrmann pyramid" formed in dual Bragg diffraction of a single crystal, where a small angular change of the incident beam is magnified to span the entire pyramid base[67]. In a sense, the single crystal acts like a lens that can magnify the object by hundreds to thousands of times depending on the experimental setup. Compared to the more popular x-ray imaging method using zone-plate lens (see Figure 1)[68], this method doesn't need the nano-fabricated lens (zone plate) that is very challenging to fabricate. However, in the work published by Xu's group, they used very large (many micrometers) gold structures as the imaging object to demonstrate the capability of x-ray imaging using a single crystal as "lens". Thus our goal is to fabricate nanoscale gold structures supported by a thin membrane (with negligible x-ray absorption) as an object in order to examine the high resolution imaging capabilities of this method.

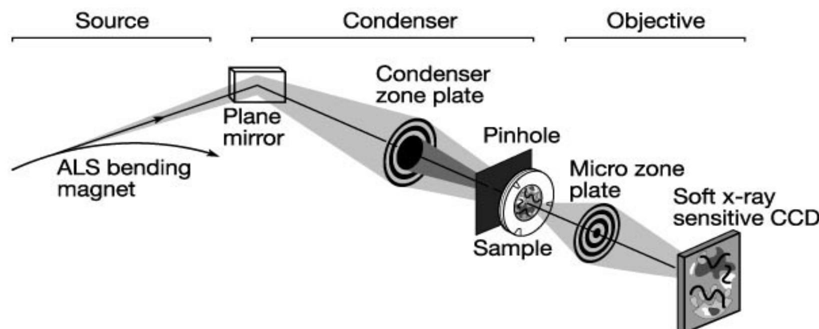


Figure 6-1: The popular x-ray imaging method using zone-plate lens.

### 6.2 X-Ray Imaging by Borrmann Pyramid

Here we briefly introduce the imaging principle. More details can be found in Xu's paper. Following the dynamic theory of x-ray scattering, when a plane wave hits a crystal it excites a pair of points on the dispersion surface, each producing a wave field traveling inside the crystal, with its energy (Poynting's vector) flowing in the normal direction to that branch of the surface. A divergent beam, which can be treated as a coherent superposition of plane waves with a continuous range of wave vectors, excites many points on the dispersion surface simultaneously, leading to the phenomenon of the Borrmann fan. When more than one set of atomic planes are excited at the same time, multiple Bragg diffraction takes place, and the Borrmann pyramid results. As shown in Figure 6-2, three triangles can be observed simultaneously on a single frame when two sets of atomic planes of a beryllium single crystal are excited. In the vicinity of the Bragg diffraction, as an incoming beam changes its incident angle over a very small range that covers the curved part of the dispersion surface, corresponding to the Darwin width which is typically about $10^{-5}$ arc, the wave fields inside the crystal will change their propagation direction by several tens of degrees ($2\theta$). This leads to a huge angular magnification. Thus, without using a zone-plate, x-ray beam manipulation can be achieved by Borrmann pyramids, where the wave front from a micrometer pinhole is propagated to become a 2+ millimeter triangle, and the size can be larger if a thicker crystal is used.

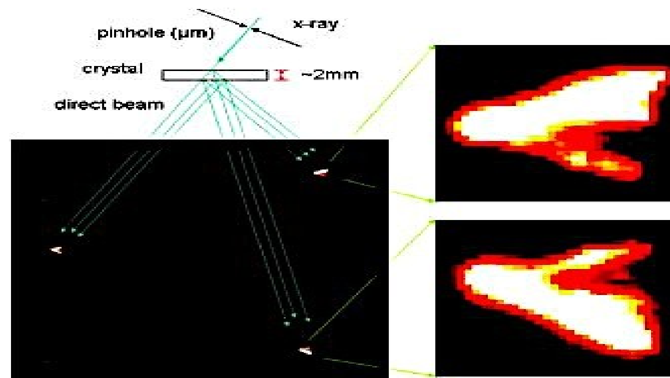


Figure 6-2: Three triangles can be observed simultaneously on a single frame when two sets of atomic planes of a beryllium single crystal are excited.

### 6.3 Structure Design and its Fabrication

The role of the object is to modulate the x-ray beam. Ideally the x-ray can pass with 100% transmission through the area not covered by Au nanostructure, and get blocked with 0% transmission in the area covered by Au nanostructure. A thin membrane made of ~100 nm-thick silicon nitride has nearly 100% transmission due to the low atomic number of Si and N. The absorption of gold by x-ray is shown in Figure 6-3. For x-ray wavelength of ~1 Å, its energy is $1.24\times10^4$ eV, leading to an absorption coefficient of ~0.3 $\mu m^{-1}$. That is, for 1 µm thick gold, the transmission would be $e^{-1\times0.3}$=74%, which is far from ideal case, but is acceptable.

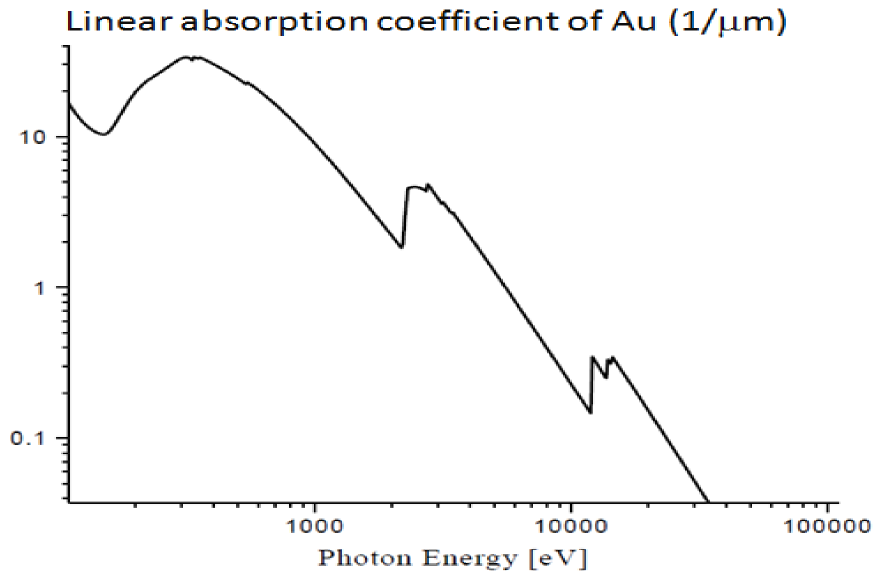


Figure 6-3: Linear absorption coefficient of Au.

To fabricate the structure as shown in figure 6-4, there are two major steps: fabrication of membrane, and fabrication of gold structure by electron beam lithography and gold electroplating (the gold structure is too high for conventional liftoff process).

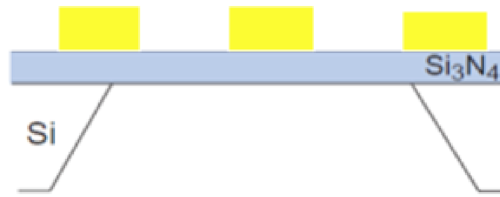


Figure 6-4: The structure to be fabricated consisting of Au nanostructure (periodic array with 600 nm pitch) on top of a silicon nitride membrane.

## 6.4 Fabrication of Silicon Nitride Membrane

### 6.4.1 Fabrication Principle

KOH etch of silicon is anisotropic. Orientation selective etch of silicon occurs in hydroxide solutions partly because of the closer packing of some orientations relative to other orientations. For silicon, the density of planes (number of Si atoms per unit area on that plane) follow: <111> > <110>, <100>; and as a result, the etching rate R follows: R (111) << R (110), R (100). Using hot aqueous KOH as etchant, the etching rate of (111) plane is several hundreds time slower than other major crystal planes (notably (100) and (110)). The etching is reaction rate limited, thus the etch rate can be controlled by varying the temperature of the solution. On the other hand, KOH etching of $Si_3N_4$ is 10000× slower than etching of silicon, thus $Si_3N_4$ is an ideal etch mask for this process.

### 6.4.2 Fabrication Steps

Figure 6-5 shows the schematic fabrication process with description of each step. Usually a photolithography step is employed to pattern the nitride layer on the back side of the wafer. To avoid this step that leads to some contamination on the front side of the wafer during spin-coating photo-resist on the back side, we designed a metal mask (Figure 6-6) that is just put on top of the wafer to etch the pattern into the silicon nitride on the back side.

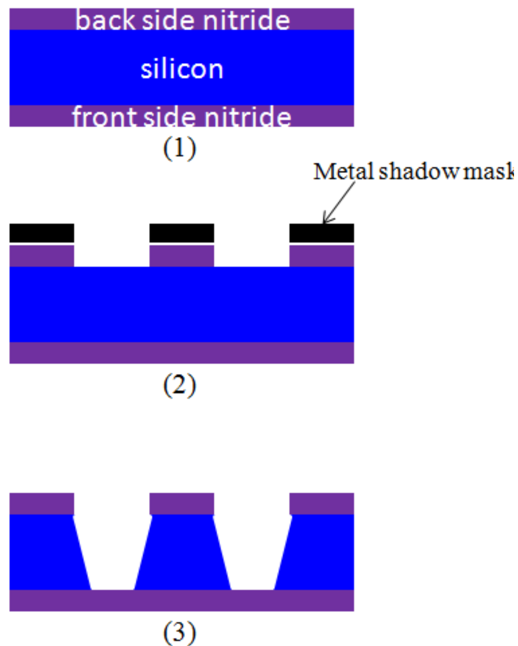


1) Low stress $Si_3N_4$ thin film is grown by LPCVD (low pressure chemical vapor deposition) on a 4-inch (100) Si wafer.

2) A metal shadow mask is used to pattern $Si_3N_4$ membranes by RIE. The etching condition is: (power, pressure, gas flow, time)

3) Anisotropic wet etching using KOH to remove silicon not protected by $Si_3N_4$ till the etching reached the front $Si_3N_4$ when the etching will be stopped. We used 30% KOH solution heated up to 80-90$^{o}$C, and the etch typically takes 3 hours.

Figure 6-5: Silicon nitride membrane fabrication process.

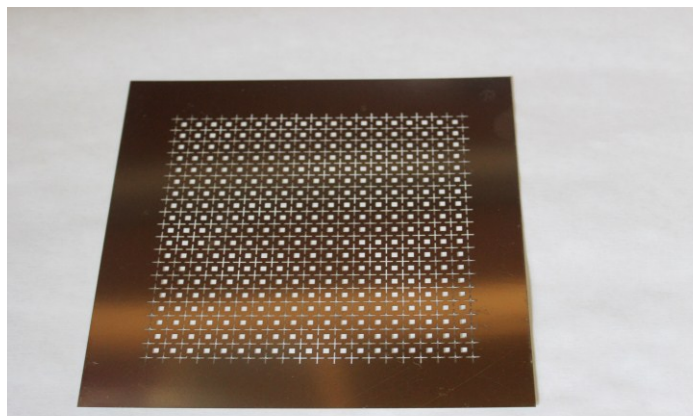

Figure 6-6: Photo of the metal shadow mask. Each repeating cell has a size of 5 mm, and the opening is 1.5 mm by 1.5 mm.

### 6.4.3 Fabrication Results

Figure 6-7 shows the fabricated silicon nitride membrane. Each membrane can be broken off the wafer easily using the etched deep trench on the back side.

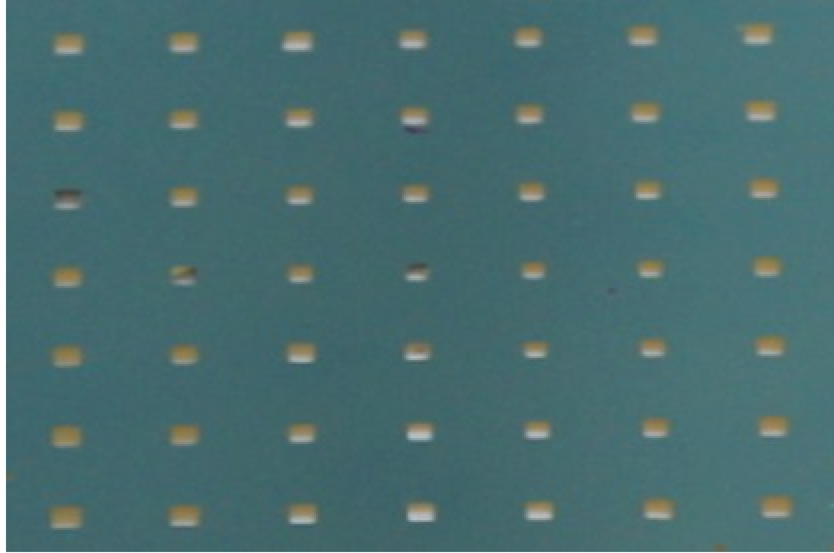

Figure 6-7: $Si_3N_4$ membrane etched on a (100) silicon wafer using KOH etch. The array periodicity is 5 mm.

### 6.5 Fabrication of Au Nanostructure on Membrane

#### 6.5.1 Gold Electroplating

Before going to the details of the fabrication process, I would like to describe gold electroplating.

##### 6.5.1.1 Advantage of Electro-Deposition

The main advantage for electroplating is low cost and high material use. For evaporation most gold is coated onto chamber wall, leading to high waste. More importantly, electro-deposition is a conformal process, that is, the structure will follow the shape of the polymer pattern (see Figure 6-8); for evaporation, and the opening will be closed gradually, leading to pyramid shape even if the hole has a cylinder shape.

##### 6.5.1.2 Electroplating Setup and Experimental Details

The conductive plating base film consists of 10 nm titanium (adhesion layer) /10 nm platinum (active layer for electroplating) on Si substrate, and the film is cleaned right before electroplating by $O_2$ plasma (20W, 20Sccm O2, 50 mtorr, 20Sec). The electroplating contains the following steps:

1- Heat 100 ml of the gold plating solution to 60 degree
2- Connect the cathode of the voltage source to the sample using alligator clip
3- Connect the anode to a 100 ohm resistor (in order to measurement current by measuring voltage drop across this resistor, I=V/R)
4- Connect the other end of the resistor to a piece of stainless steel
5- Place the sample (cathode) and the piece of stainless steel (counter electrode) in the solution
6- Turn on the voltage source and apply 1.5 V
7- Use the multimeter to verify that the voltage across the solution is 1.4 V
8- Plate for 5 minutes

The I-V curve of the electroplating solution is shown in Figure 6-9. Higher voltage leads to higher current and higher plating rate, but more hydrogen generation. To reduce hydrogen bubble generation, we reduced the voltage to 1.5V. At this voltage, the current density is 0.8 mA/cm$^2$.

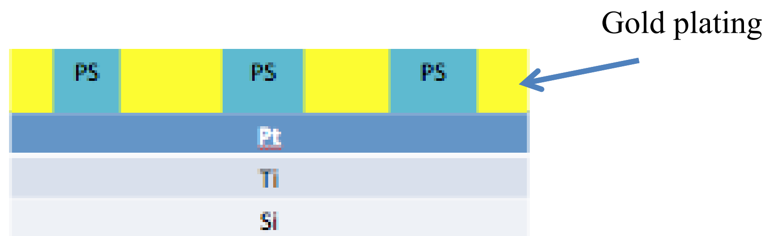


Figure 6-8 Schematic representation of electroplating process to fill holes in the resist.

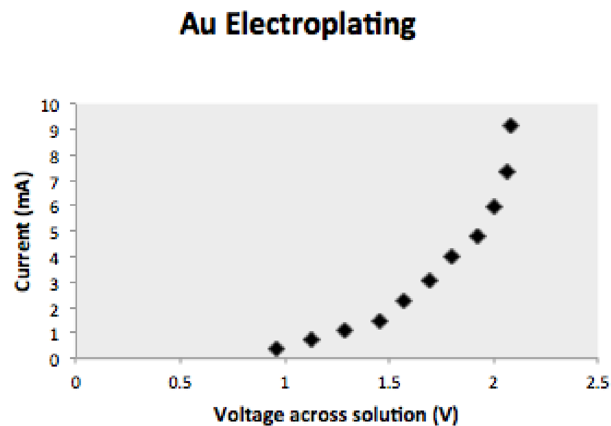

Figure 6-9: I-V curve of the gold electroplating solution (by Golam Bappi).

We calculated the theoretical plating rate of Au (nm/sec) assuming 5mA/in$^2$ current. Assume one electron is needed to reduce each Au ion into Au atom, with Au density as 19.3g/cm$^3$, the plating rate is calculated as 50nm/min. If assuming each Au ion needs 3 electrons to be reduced to form Au atom, the rate would be 1/3, or 16.7nm/min, which is close to our experimental result (140nm over 20min). Thought the plating rate is low, we can deposit 1000 nm Au within three hours.

#### 6.5.1.3 Results of Electroplating

Figure 6-10 shows the photo of silicon wafer pieces with electro-deposited Au to have a uniform film obtained by electroplating for 5min.

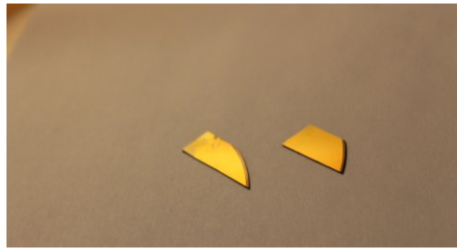

Figure 6-10: Photo of two pieces of wafer with electroplated gold on the Pt conducting layer.

### 6.5.2 Gold Structure Fabrication Steps Using a Single Layer Resist

The fabrication process steps are shown and described in Figure 6-11.

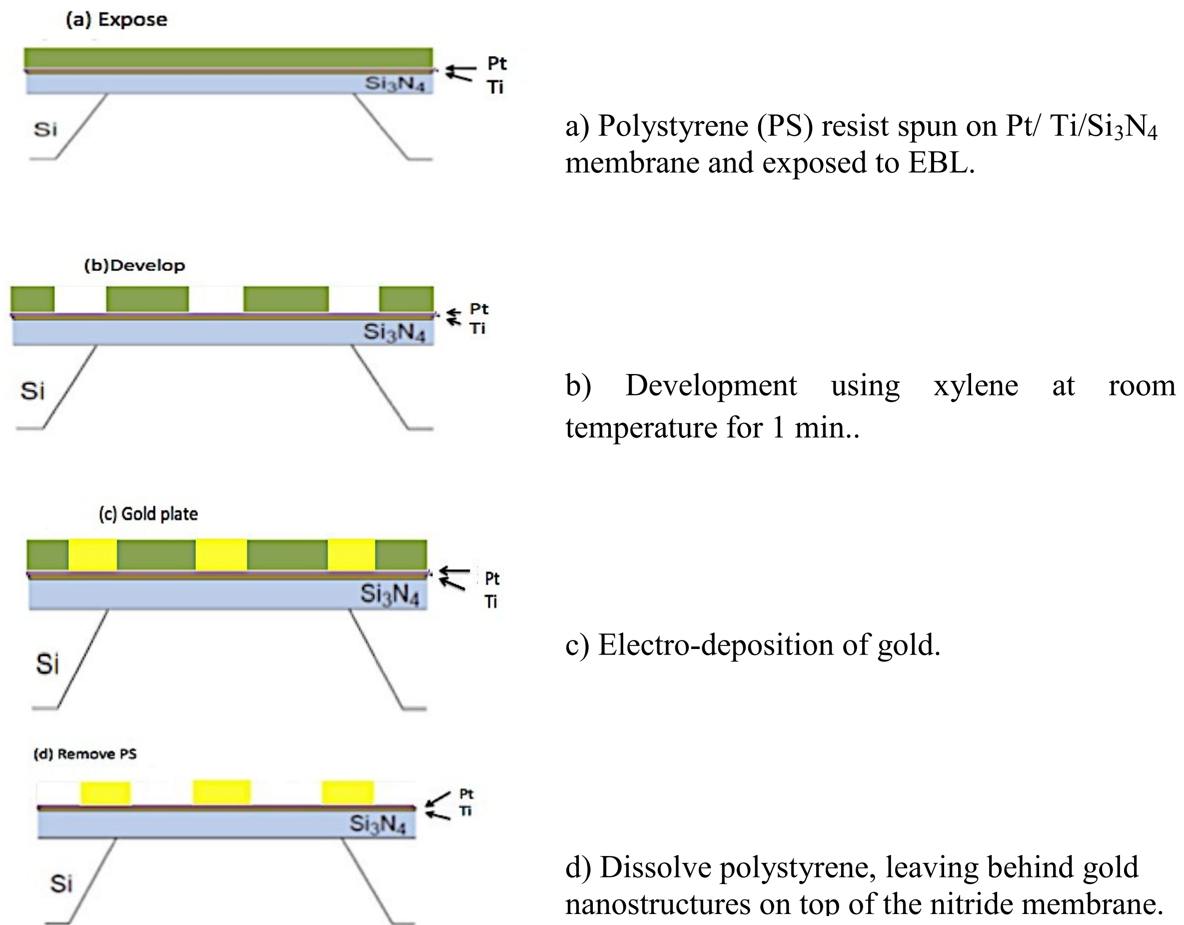


Figure 6-11: Fabrication process steps using a single layer resist

### 6.5.2.1 Results Using a Single Layer Resist

We dissolved 260Kg/mol high molecular weight of polystyrene in chlorobenzene to make a 10 wt/vol % solution that gave a 1.27 $\mu$m film by spin-coating at 1300 rpm on 10nm Ti and 10nm Pt layers coated by electron beam evaporator on top of membrane. The film was then baked on a hotplate at 150$^{o}$C for 5 min. After exposure at 20 keV using Raith 150 $^{TWO}$ electron beam lithography system, the resist was developed in xylene for 2 min at room temperature, followed by rinsing the wafer by 2-propanol and drying. As seen in Figure 6-12,the pattern collapsed due to capillary force during developer drying.

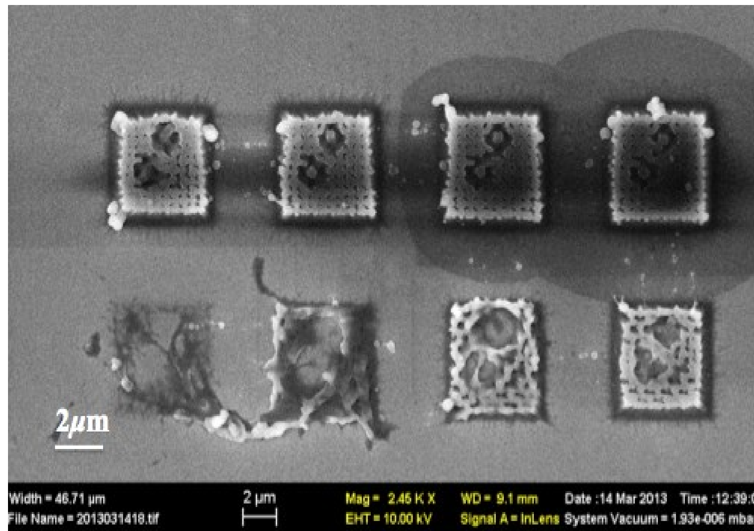


Figure 6-12: SEM images polystyrene pattern on membrane showing collapsed patterns due to capillary force.

### 6.5.3 Fabrication Step Using Tri-Layer Stack

To solve the pattern collapse issue we used tri-layer polymer film stack on membrane as following:

- 1- 1 $\mu$m PMMA
- 2- 15 nm Al
- 3- 100 nm polystyrene.

And the fabrication process is shown in Figure 6-13. Here the top layer polystyrene is very thin, thus the low-aspect ratio polystyrene pattern after development is not likely to collapse. The high aspect ratio pattern in PMMA is etched by RIE, without any liquid involved in the process hence the absence of capillary force,

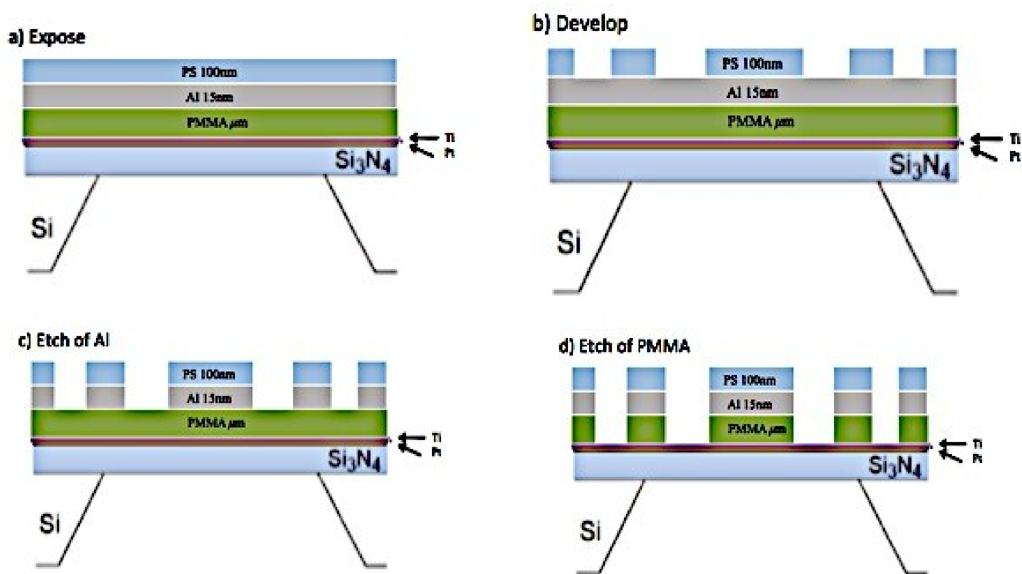


Figure 6-13: Fabrication process using tri- layer stack to create the polymer matrix for subsequent gold electroplating.

In the experimental 1 $\mu$m PMMA film was obtained by spin coating at 4000rpm on membrane. The film was baked on a hotplate at 120$^{o}$C for 10 min. After that, 15 nm of Al was coated by electron beam evaporation, followed by spinning polystyrene of 100 nm thickness which was subsequently baked at 90$^{o}$C for 10 min.

As expected, thinner PS layer was found to have no pattern collapse. The exposure at 20 keV using Raith 150 $^{TWO}$ electron beam lithography system was conducted, and the resist was developed in xylene for 2 min at room temperature followed by rinsing the wafer by 2-propanol. Next, a short etching by using $O_2$ plasma was carried out to remove any possible residual, and then the pattern was transferred to the underlying Al and PMMA layers consecutively using RIE.

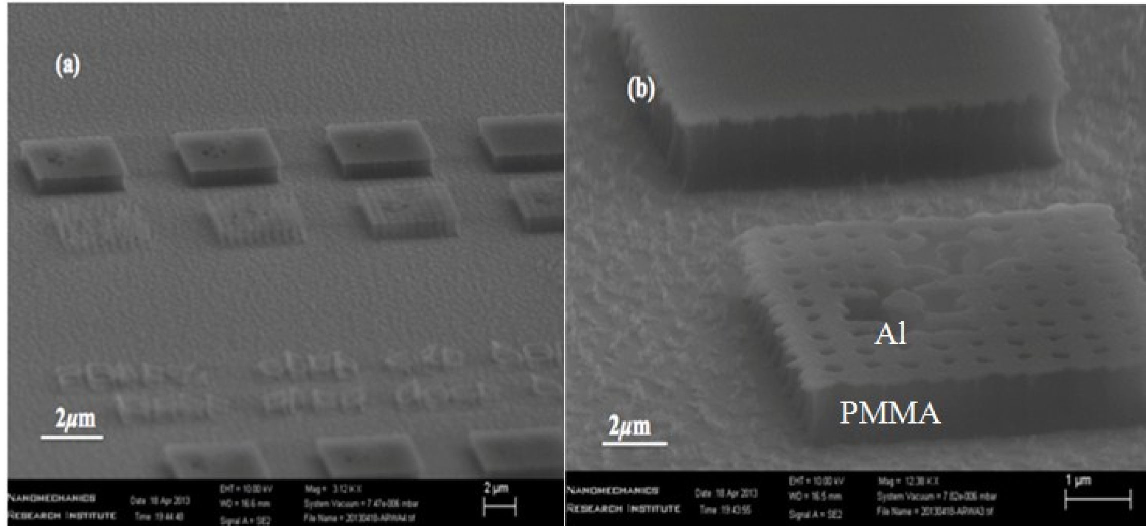


Figure 6-14: SEM images of the result after pattern transfer into the tri-layer stacks.

Figure 6-14 shows the SEM image after pattern transfer into the thick PMMA layer. For too low exposure dose (Figure 6-14a lower left), the PS is not fully cross-linked and thus the underneath Al is etched away, resulting in shallow or no patterns. Whereas for too high doses (Figure 6-14b top), all the PS is cross-lined due to direct or proximity exposure, leading to a large thick block of PMMA without any pattern. At present, the remaining issue to solve is the rough residual on the bottom and electroplating of gold into the pattern.

### 6.5.4 Conclusion

We explored the fabrication of gold structure on a thin membrane, which will be used as an object for novel x-ray imaging. We developed the fabrication process for silicon nitride membrane, electroplating of gold, and pattern transfer after electron beam lithography using single layer resist and tri-layer resist stack.

# Appendix: List of Publications

**Journal Papers**

[1] A. S. Abbas, M. Yavuz and B. Cui. 2013. Polycarbonate as an ideal grayscale electron beam resist using diluted cyclopentanone developer. Microelectronic Engineering MEE-D-13-00418.

[2] C. Con, A.S. Abbas, M. Yavuz and B. Cui. 2013. Dry Thermal Development of Negative Electron Beam Resist Polystyrene. Advances in Nano Research, *An International Journal*, **1**, 2.

[3] A. S. Abbas, M. Yavuz and B. Cui. 2013. Metal nanostructure fabrication by electron beam lithography and dry liftoff, manuscript under preparation.

[4] A. S. Abbas, M. Yavuz and B. Cui. 2013. Water soluble and developable electron beam resist PSS, manuscript under preparation.

**Conference Presentations**

[1] C. Con, A. S. Abbas, M. Yavuz and B. Cui. May 2012. Dry Thermal Development of Negative Electron Beam Resist Polystyrene. EIPBN, 56th, International Conference on Electron, Ion and Photon Beam and Nanofabrication, Waikoloa, Hawaii.

[2] A. S. Abbas, M. Yavuz and B. Cui. May 2013 Polycarbonate as an ideal grayscale electron beam resist using diluted cyclopentanone developer. EIPBN, 57th, International Conference on Electron, Ion and Photon Beam and Nanofabrication, Nashville, Tennessee.

[3] A. S. Abbas, M. Yavuz and B. Cui. September 2013. Metal nanostructure fabrication by electron beam lithography and dry liftoff. 39th International Conference on Micro and Nano Engineering, London, UK.

[4] A. S. Abbas, M. Yavuz and B. Cui. September 2013. Water soluble and developable electron beam resist PSS. 39th International Conference on Micro and Nano Engineering, London, UK.

# Bibliography


[1] Tseng, A. A. 2008. Nanofabrication: Fundamentals and Applications. World Scientific Publishing Company.

[2] Ugo, P. and Moretto, L. M. 2007.Handbook of Electrochemistry.Zoski, C. (Ed) (Amsterdam: Elsevier), p. 678.

[3] Menon, V. P. and Martin, C. R. (1995) *Analytical Chemistry,***67**, (1920).

[4] Moretto, L. M., Tormen, M.De Leo, M., Carpentiero, A. and Ugo, P. 2011.Polycarbonate-based ordered arrays of electrochemical nanoelectrodes obtained by e-beam lithography. *Nanotechnology,***22**,185305, (7pp), doi:10.1088/0957-4484/22/18/185305.

[5] Madou, M. J. 2002. Fundamentals of Microfabrication: the science of miniaturization: CRC Press.

[6] Yang, J. K. W., Jung,Y. S., Chang, J., Mickiewicz, R. A.,Alexander-Katz, A., Ross, C. A., and Berggren,K. K. 2010. Complex self-assembled patterns using sparse commensurate templates with locally varying motifs. *Nature Nanotechnology,* **5**, 256.

[7] Ji,S., Liu,C., Liu,G., and Nealey, P. F. 2010. Molecular transfer printing using block copolymers. *ACS Nano,***4**, 599.

[8] Geissler, M., and Xia, Y. 2004. Patterning: principles and some new developments. *Advance Material,* **16** (15), 1249-1269.

[9] Mohammad, M. A., Fito, T., Chen, J., Buswell, S., Aktary, M., Dew, S. K., and Stepanova,M. 2010.In: Lithography, Michael Wang (Ed.) 293, (INTECH).

[10] Mohammad, M. A., Mustafa, M., Dew, S. K., Stepanova, M. 2012.The Interdependence of Exposure and Development Conditions when Optimizing Low-Energy EBL for Nano-Scale Resolution In: Nanofabrication Techniques and Principles, M. Stepanova and S. Dew (Eds.), 350, (Springer).

[11] Cui B. (n.d.). Retrieved from https://ece.uwaterloo.ca/~bcui/ECE_730.html

[12] Cui Z. (n.d.). Nanofabrication: principles, capabilities and limits.

[13] Stepanova, M., Fito, Z., Szabo,T., Alti, K., Adeyenuwo,A. P., Koshelev, K., Aktary, M., and Dew, S. K. 2010.Simulation of electron beam lithography of nanostructures, *Journal of Vacuum Science and Technology B,***28**, C6C48.

[14] Mohammad,M.A., Dew, S.K., Westra,K., Li,P., Aktary,M., Lauw,Y., Kovalenko, A., and Stepanova, M. 2007. Nanoscale resist morphologies of dense gratings using electron-beam lithography. *Journal of Vacuum Science and Technology B,***25**, 745.

[15] Fischer, P. B. 1993. Ph. D. thesis. Retrieved from University of Minnesota.

[16] Anner, GE. 1990.Planar Processing Primer: Van Norstrand Reinhold

[17] Charlesby, A. 1960. Atomic radiation and polymers. London: Pergamon.

[18] I Zailer, J E F Frost, V Chabasseur-Molyneux, C J B Ford and M Pepper. 1996. Crosslinked PMMA as a high-resolution negative resist for electron beam lithography and applications for physics of low-dimensional structures, Semicond. Sci. Technol. 11, 1235–1238.

[19] Pease, R. F. W. 1981.Electron Beam Lithography.*Contemporary Physics,***22**, 265.

[20] Reimer, L. 1989.Transmission Electron Microscopy. New York:Springer-Verlag.

[21] Leibmann, G. 1955. A unified representation of magnetic electron lens properties. *Proceeding of the Physical Society B,***68**, 737.

[22] Krauss,P. R. 1997. Ph. D. Thesis. Retrieved from University of Minnesota.

[23] Mackie, S. and Beaumont,S. P. 1995.Solid State Technology, P. 117.

[24] H. G, Craighead, R. E. Howard, L. D. Jackel, and P. M. Mankiewich. 1983. 10‐nm linewidth electron beam lithography on GaAs, Appl. Phys. Lett. **42 (1)**, 38.

[25] Chang, T. H. P. 1975. Proximity effect in electron-beam lithography.*Journal of Vacuum Science and Technology,***12**, 1271.

[26] Richston, S. A., and Kern, D. P. 1987. Point exposure distribution measurements for proximity correction in electron beam lithography on a sub-100 nm scale.*Journal of Vacuum Science and Technology B,***5**, 135.

[27] Wiederrecht G. 2010. Handbook of nanofabrication, Elsevier

[28] Tanenbaum,D. M., Lo,C. W., Isaacson, M., Craighead, H. G., Rooks,M. J., Lee, K. Y., Huang,W. S., and Chang,T. H. P. 1996. High resolution electron beam lithography using

ZEP - 520 and KRS resists at low voltage, *Journal of Vacuum Science and Technology B,***14**, 3829.

[29] Yang, H., Fan, L., Jin,A., Luo,Q., Gu,C., and Cui, Z. 2006.*Proc. 1st IEEE-NEMS,* 60501014, **391**.

[30] Mohammad , M. 2012. Study of development processes for zep-520 as a high-resolution positive and negative tone electron beam lithography resist. *Japanese Journal of Applied Physics,***51**, 06FC05.

[31] Koshelev, K. Mohammad. M, Fito,T. 2011. Comparison between ZEP and PMMA resists for nanoscale electron beam lithography experimentally and by numerical modeling, *Journal of Vacuum Science and Technology B,* **29**, 06F306-1.

[32] Ku, H. Y. and Scala, L. C. 1969. Polymeric electron beam resists. Journal of *ElectrochemicalSociety,* **116**, 980-985.

[33] Bilenberg, B., Schøler, M., Shi, P., Schmidt, M. S., Bøggild, P., Fink, M., Schuster, C., Reuther, F., Gruetzner, C., Kristensen, A. 2006. Comparison of high resolutionnegative electron beam resists. *Journal of Vacuum Science and Technology B,***24**(4), 1776-1779.

[34] S. Ma, Con, C., Yavuz, M., and Cui, B. 2011. Polystyrene negative resist for high resolution electron beam lithography. *Nanoscale research letters,***6**,446.
doi: 10.1186/1556-276X-6-446.

[35] H. Namatsu. 2000. Supercritical resist dryer, J. Vac. Sci. Technol. B **18**[6] 3308.

[36] H. Namatsu . 2004. The Impact of Supercritical Fluoro-Compounds on Lithography Use, Jpn. J. Appl. Phys., **43**[4A] L456.

[37] T. Wahlbrink, Daniel Küpper, Y.M. Georgiev, J. Bolten, M. Möller, David Küpper, M.C. Lemme, H. Kurz. 2006.Microelectron, Supercritical drying process for high aspect-ratio HSQ nano-structures, Eng.**83**, 1124.

[38] T. Tanaka, M. Morigami, H. Oizumi, and T. Ogawa. 1993.Freeze-Drying Process to Avoid Resist Pattern Collapse, Jpn. J. Appl. Phys. **32**, 5813.

[39] V. Auzelyte, A. Langner and H. H. Solak. 2009. Thermal development of a calixarene resist, J. Vac. Sci. Technol. B, **27**[6] 2990.

[40] D. A. Z. Zheng, M. A. Mohammad, S. K. Dew and M. Stepanova. 2011. Developer-free direct patterning of PMMA/ZEP 520A by low voltage electr on beam lithography, J. Vac. Sci. Technol. B, **29**[6] 06F303.

[41] D. G. De Oteyza, P. N. Perera, M. Schmidt, M. Falch, S. D. Dhuey, B. D. Harteneck, A.M. Schwartzberg, P. J. Schuck, S. Cabrini, and D. L. Olynick. 2012. Sub-20 nm laser ablation for lithographic dry development, Nanotechnol. **23**[18] 185301.

[42] C. Con, R. Dey, M. Ferguson, J. Zhang, R. Mansour, M. Yavuz, and B. Cui. 2012. High molecular weight polystyrene as very sensitive electron beam resist , *Microelectron. Eng.***98**, 254.

[43] R. Dey and B. Cui. 2013. Effect of molecular weight distribution on e-beam exposure properties of polystyrene, Nanotechnology, 24 245302.

[44] T. Dillon, M. Zablocki, J. Murakowski and D. Prather, Processing and modeling optimization for grayscale lithography, Proc. of SPIE **6923**, 69233B.

[45] A. Schleunitz, V. A. Guzenko1, A. Schander, M. Vogler and H. Schift. 2011. Selective profile transformation of electron-beam exposed multilevel resist structures based on a molecular weight dependent thermal reflow, J. Vac. Sci. Technol. B **29**, 06F302.

[46] H. A. Bethe, M. E. Rose, and L. P. Smith. 1938. Proceedings, American Philosophical Society **78**,583.

[47] K. Kanaya and S. Okayama. 1972. Penetration and energy-loss theory of electrons in solid targets, J. Phys. D: Appl. Phys. **5**, 43.

[48] M. A. Mohammad, K. Koshelev, T. Fito, D. Ai Zhi Zheng, M. Stepanova, and S. Dew. 2012.Study of Development Processes for ZEP-520 as a High-Resolution Positiveand Negative Tone Electron Beam Lithography Resist, Jpn J. Appl. Phys **51**, 06FC05.

[49] A. E. Grigorescu and C. W. Hagen. 2009. Resists for sub-20-nm electron beam lithography with a focus on HSQ: state of the art, Nanotechnology. 20, 292001.

[50] A. A. Tseng, J. 2004. Recent developments in micromilling using focused ion beam technology, Micromech. Microeng. **14,** R15.

[51] H. Schift. 2008. Nanoimprint lithography: An old story in modern times? A review, J. Vac. Sci. Technol. B, **26,** 458.

[52] L. E. Ocola and A. Stein. 2006. Effect of cold development on improvement in electron-beam nanopatterning resolution and line roughness, J. Vac. Sci. Technol. B, **24,** 3061.

[53] P. Appel. 2001.Track etching technique in membrane technology, Radiation Measurements. **34,** 559–566.

[54] G. B. Nash. 1990. Filterability of blood cells: methods and clinical applications, Clin. Hemorheol. **10,** 353–362.

[55] S. K. Chakarvarti. 2009. Track-etch membranes enabled nano-/microtechnology: A review, Radiation Measurements. **44,** 1085–1092.

[56] F. Muench, M. Oezaslan, T. Seidl, S. Lauterbach, P. Strasser, H.-J. Kleebe, and W. Ensinger. 2011. Multiple activation of ion track etched polycarbonate for the electroless synthesis of metal nanotubes, Appl. Phys. A, **105,** 847–854.

[57] M. E. Toimil Molares, J. Brötz, V. Buschmann, D. Dobrev, R. Neumann, R. Scholz, I. U. Schuchert, C. Trautmann, and J. Vetter. 2001. Etched heavy ion tracks in polycarbonate as template for copper nanowires, Nucl. Instr. Meth. Phys. Res. B, **185,** 192-197.

[58] L. M. Moretto, M. Tormen, M. De Leo, A. Carpentiero, and P. Ugo. 2011. Polycarbonate-based ordered arrays of electrochemical nanoelectrodes obtained by e-beam lithography, Nanotechnology. **22,** 185305.

[59] A. Schleunitz, V. A. Guzenko1, A. Schander, M. Vogler, and H. Schift. 2011. Selective profile transformation of electron-beam exposed multilevel resist structures based on a molecular weight dependent thermal reflow, J. Vac. Sci. Technol. B, **29,** 06F302.

[60] H. Tsai, H. Smith, and R. Menon. 2007. Fabrication of spiral-phase diffractive elements using scanning-electron-beam lithography,J. Vac. Sci. Technol. B, **25,** 2068-2071.

[61] M. Yan, S. Choi, K. R. V. Subramanian, and I. Adesida. 2008. The effects of molecular weight on the exposure characteristics of poly (methylmethacrylate) developed at low temperatures, J. Vac. Sci. Technol. B, **26,** 2306.

[62] B. Bilenberg, S. Jacobsen, M. S. Schmidt, L. H. D. Skjolding, P. Shi, P. Boggild, J. O.Tegenfeldt, and A. Kristensen. 2006. High resolution 100kV electron beam lithography in SU-8,Microelectronic. Eng. **83,** 1609-1612.

[63] A. S. Abbas, M. Yavuz and B. Cui. 2013. Polycarbonate as an ideal grayscale electron beam resist using diluted cyclopentanone developer, submitted to Microelectronic Engineering MEE-D-13-00418.

[64] Stanford Nanofabrication Facility. 2013. Lift-off. Retrieved from, https://snf.stanford.edu/SNF/processes/process-modules/photolithography/lift-off-lol-procedures/liftoff

[65] S. Ma, C. Con, M. Yavuz and B. Cui. 2011.Polystyrene negative resist for high-resolution electron beam lithography,Nanoscale Res. Lett. 6, 446.

[66] A. Elschner, S. Kirchmeyer, W. Lovenich, U. Merker, K. Reuter. 2010. PEDOT: Principles and Applications of an Intrinsically Conductive Polymer, CRC Press, Boca Raton, FL, USA.

[67] G. Xu and J. Britten. 2008. Modulation of hard x-ray beam profiles by Borrmann pyramid, J. Appl. Phys. 103, 023509.

[68] W. Chao, B. D. Harteneck, J. A. Liddle, E. H. Anderson, and D. T. Attwood. 2005. Soft X-ray microscopy at a spatial resolution better than 15 nm, Nature 435, 1210-1213.